Nonsmooth analysis of the impact between successive skew bridge-segments

Elias G. Dimitrakopoulos

Nonlinear Dynamics
An International Journal of Nonlinear Dynamics and Chaos in Engineering Systems

ISSN 0924-090X
Volume 74
Number 4

Nonlinear Dyn (2013) 74:911-928
DOI 10.1007/s11071-013-1012-7

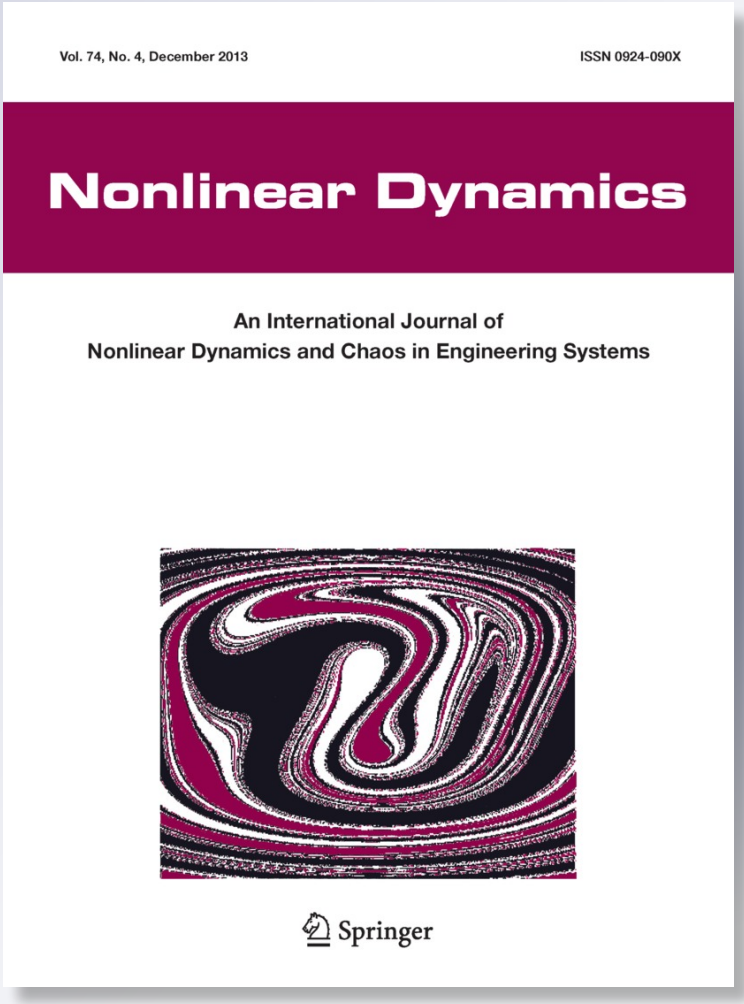

Springer

Nonlinear Dyn (2013) 74:911–928
DOI 10.1007/s11071-013-1012-7

ORIGINAL PAPER

Nonsmooth analysis of the impact between successive skew bridge-segments

Elias G. Dimitrakopoulos

Received: 23 February 2013 / Accepted: 16 July 2013 / Published online: 23 August 2013

Abstract Skew bridges with in-deck joints belong to the most common types of existing bridges worldwide. Empirical evidence from past earthquakes indicates that such, multi-segment, skew bridges often rotate in the horizontal plane, increasing the chances of deck unseating. The present paper studies the oblique in-deck impact between successive bridge segments, which triggers this peculiar rotation mechanism. The analysis employs a nonsmooth rigid body approach and utilizes set-valued force laws. A key feature of this approach is the *linear complementarity problem* (LCP) which encapsulates all physically feasible post-impact states. The LCP results in pertinent closed-form solutions which capture each of these states, and clarifies the conditions under which each post-impact state appears. In this context, a rational method to avoid the singularities arising from dependent constraints is coined. The results confirm theoretically the observed tendency of skew (bridge deck) segments to bind in their obtuse corners and rotate in such a way that the skew angle increases. Further, the study offers equations which describe the contact kinematics between two adjacent skew planar rigid bodies. The same equations can be used to treat successively as many pairs of skew bridge-segments as necessary.

E.G. Dimitrakopoulos (✉)
Department of Civil and Environmental Engineering,
The Hong Kong University of Science and Technology,
Clear Water Bay, Kowloon, Hong Kong
e-mail: ilias@ust.hk

Keywords Skew bridges · Oblique impact · Unilateral contact · Concrete bridges · Linear complementarity problem · Nonsmooth dynamics

1 Introduction

The present paper focuses on the earthquake-induced impact between adjacent skew bridge deck segments. It extends previous work of the author, which concerned skew bridges with solely deck-abutment expansion joints, to the case of skew bridges with in-deck joints. On the same time, this paper derives from a broader study [1–3] on the problem of earthquake-induced pounding in bridges.

The peculiar seismic response of skew bridges has been reported systematically after the 1971 San Fernando earthquake [4–6], and continues to attract the attention of researchers ever since (e.g. [7–11] and references therein). During earthquake excitation, adjacent skew deck-segments often bind in one of the obtuse corners and rotate, in the horizontal plane, in the direction of increasing the skew angle [12, 13] (Fig. 1). This coupling of the longitudinal and the transverse response, is primarily triggered by oblique impact at the expansion joints and increases the tendency of the deck to drop off the supports [12, 14]. Two cases are distinguished from a kinematical point of view: (a) the "deck-abutment" contact (examined in [1]) and (b) the more complicated, "in-deck" contact between adjacent skew bridge segments (Fig. 1), which is the focus of

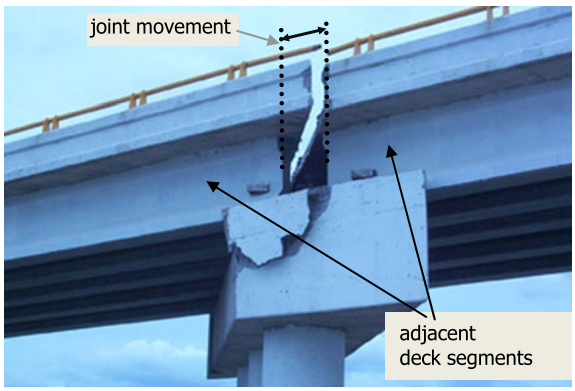

Fig. 1 Damage of a skew bridge after the Tehuacan 1999 Mexico earthquake (adapted from [25])

the present paper. The latter might occur during the seismic response of bridges with in-deck joints (multi-segment deck).

Despite the dominant role of pounding on the seismic response of straight (see [15–17] and references therein) and particularly of skew bridges, there is a lack of experimental results and/or field measurements that would shed light on the pounding-induced rotations. Instead, most studies rely on a numerical simulation of the associated contact/impact, adopting the contact element (or "compliance") approach. The deck-abutment impact has been modelled with a single unilateral spring activated only in compression ("gap" element) [18, 19], and more recently, with multiple distributed gap elements aligned perpendicularly to the contact surface [7, 20, 21]. For the same type of impact, Maleki [22] used a gap element at the acute corner and a "hook" element (a unilateral spring working only in tension) at the obtuse corner of the deck. Similarly, the in-deck contact/impact is simulated with either single gap elements at the corners of the individual deck segments [23, 24] or with distributed gap elements along the contact surface, as in the detailed study of Huo and Zhang [14].

Nonsmooth dynamics [26–30] offers an alternative simulation approach of the earthquake-induced pounding in bridges. Within this context, contact and impact are treated as inequality problems, for instance *linear complementarity problems* (LCP) and impact laws often assume a set-valued form [1, 27, 31, 32]. The author proposed such a framework for the earthquake-induced pounding in straight [2, 16] and in skew bridges with solely deck-abutment joints [1, 33].

The work reported herein extends the previous work of the author [1] as: (a) it deals with the general, from a kinematical point of view, case of pounding in skew bridges, (b) it proposes a rational way to avoid singularities (singular matrices) caused by dependent constraints, and (c) offers original closed-form solutions for the in-deck impact of skew bridges. The motivation for this study originates from: (i) the need to elucidate the oblique impact phenomenon in skew bridges with in-deck joints, (ii) the importance of this rotation mechanism manifested by empirical evidence, and (iii) the large number of existing skew bridges, which, in many seismic regions worldwide, represent the majority of the bridge stock [17].

2 Proposed nonsmooth dynamics approach

This study considers the individual bridge deck segments (in-between two successive separation/expansion joints) as rigid bodies moving on the horizontal plane. The study further assumes that the interaction between adjacent segments is a unilateral contact and adopts the simplest impact laws, in a set-valued form [1, 27, 32], to describe this interaction.

In particular, a set-valued map, the unilateral primitive Upr (e.g. Fig. 2, right) and Newton's coefficient of restitution $\varepsilon_N \in [0, 1]$ describe the behavior in the normal direction of contact i:

$$-\Lambda_{Ni} \in \mathrm{Upr}(v_{Ni}) \tag{1}$$

where $v_{Ni} \doteq \gamma_{Ni}^{+} + \varepsilon_N \gamma_{Ni}^{-}$ is the associated velocity jump in the normal direction, γ_{Ni} is the relative velocity in the normal direction of impact and Λ_{Ni} is the associated impulse. Throughout this paper, superscript "+" refers to the post-impact state and superscript "−" to the pre-impact state.

A different set-valued map, the $\mathrm{Sgn}(x)$ function, enforces Coulomb's friction law in the tangential direction of contact i:

$$-\Lambda_{Ti} \in \mu_i \Lambda_{Ni}\, \mathrm{Sgn}\left(\gamma_{Ti}^{+}\right) \tag{2}$$

where μ is the coefficient of friction and Λ_{Ti} the tangential impulse. The $\mathrm{Sgn}(x)$ function differs from the standard sgn function at the point $x = 0$, where the former yields a set of values: $\mathrm{Sgn}(x = 0) = [-1, 1]$, instead of a single value $\mathrm{sgn}(x = 0) = 0$. Key role in this approach holds the decomposition (3) (Fig. 2), which restores the complementarity conditions in the tangential direction of impact:

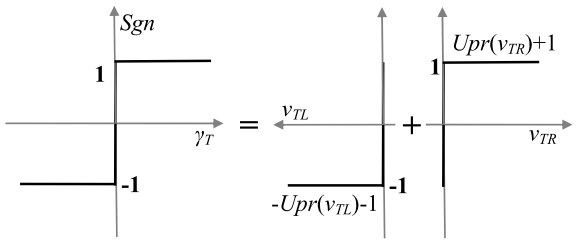

Fig. 2 Set-valued friction force law [31]

$$\begin{cases} -\Lambda_{TRi} \in \mathrm{Upr}(v_{TRi}) & \Lambda_{TRi} = \mu\Lambda_{Ni} + \Lambda_{Ti} \\ -\Lambda_{TLi} \in \mathrm{Upr}(v_{TLi}) & \Lambda_{TLi} = \mu\Lambda_{Ni} - \Lambda_{Ti} \\ \gamma_{Ti}^{+} = v_{TRi} - v_{TLi} \end{cases} \tag{3}$$

In which v_{TR} and v_{TL} are the right and left velocity-parts (Fig. 2) of the post-impact tangential velocity: $\gamma_{Ti}^{+} = v_{TRi} - v_{TLi}$ and Λ_{TR} and Λ_{TL} are the corresponding impulses.

In integrated form the Newton–Euler equations are

$$\mathbf{M}\left(\mathbf{u}^{+} - \mathbf{u}^{-}\right) = \mathbf{W}_N \boldsymbol{\Lambda}_N + \mathbf{W}_T \boldsymbol{\Lambda}_T \tag{4}$$

where $\mathbf{M}$ is the mass matrix and $\mathbf{W}$ are the direction matrices of the impulse vectors $\boldsymbol{\Lambda}$ in the normal $\mathbf{W}_N = \{\mathbf{w}_{Ni}\}$ and the tangential direction $\mathbf{W}_T$ (40), respectively; sub-indices N, T are used throughout this paper in the same sense. For the generalized velocities $\mathbf{u}$ and the generalized coordinates $\mathbf{q}$, $\dot{\mathbf{q}} = \mathbf{u}$ holds in an "*almost everywhere*" sense of functional analysis [31].

The relative (contact) velocities in the normal $\gamma_{Ni} = \mathbf{w}_{Ni}^T \mathbf{u}$ and the tangential $\gamma_{Ti} = \mathbf{w}_{Ti}^T \mathbf{u}$ direction appear by pre-multiplying (4) with $\mathbf{W}_N^T \mathbf{M}^{-1}$ and $\mathbf{W}_T^T \mathbf{M}^{-1}$:

$$\begin{aligned} \boldsymbol{\gamma}_N^{+} - \boldsymbol{\gamma}_N^{-} &= \mathbf{G}_{NN}\boldsymbol{\Lambda}_N + \mathbf{G}_{NT}\boldsymbol{\Lambda}_T \\ \boldsymbol{\gamma}_T^{+} - \boldsymbol{\gamma}_T^{-} &= \mathbf{G}_{TN}\boldsymbol{\Lambda}_N + \mathbf{G}_{TT}\boldsymbol{\Lambda}_T \end{aligned} \tag{5}$$

where the "**G**" matrices are

$$\begin{aligned} \mathbf{G}_{NN} &= \mathbf{W}_N^T \mathbf{M}^{-1} \mathbf{W}_N & \mathbf{G}_{NT} &= \mathbf{W}_N^T \mathbf{M}^{-1} \mathbf{W}_T \\ \mathbf{G}_{TN} &= \mathbf{W}_T^T \mathbf{M}^{-1} \mathbf{W}_N & \mathbf{G}_{TT} &= \mathbf{W}_T^T \mathbf{M}^{-1} \mathbf{W}_T \end{aligned} \tag{6}$$

Following the procedure outlined in [1] the problem of the frictional multi-impact is formulated as a *linear complementarity problem* (LCP):

$$\begin{pmatrix} \mathbf{v}_N \\ v_{TR} \\ \Lambda_{TL} \end{pmatrix} = \begin{pmatrix} \mathbf{G}_{NN} - \mathbf{G}_{NT}\bar{\bar{\boldsymbol{\mu}}} & \mathbf{G}_{NT} & \mathbf{0} \\ \mathbf{G}_{TN} - G_{TT}\bar{\bar{\boldsymbol{\mu}}} & G_{TT} & 1 \\ 2\bar{\bar{\boldsymbol{\mu}}} & -1 & 0 \end{pmatrix} \begin{pmatrix} \boldsymbol{\Lambda}_N \\ \Lambda_{TR} \\ v_{TL} \end{pmatrix} + \begin{pmatrix} (\bar{\bar{\varepsilon}}_N + \mathbf{E})\boldsymbol{\gamma}_N^{-} \\ \gamma_T^{-} \\ 0 \end{pmatrix} \tag{7}$$

$$\begin{pmatrix} \mathbf{v}_N \\ v_{TR} \\ \Lambda_{TL} \end{pmatrix} \geq 0, \quad \begin{pmatrix} \boldsymbol{\Lambda}_N \\ \Lambda_{TR} \\ v_{TL} \end{pmatrix} \geq 0$$
$$\begin{pmatrix} \mathbf{v}_N \\ v_{TR} \\ \Lambda_{TL} \end{pmatrix}^T \begin{pmatrix} \boldsymbol{\Lambda}_N \\ \Lambda_{TR} \\ v_{TL} \end{pmatrix} = 0 \tag{8}$$

where: $\boldsymbol{\Lambda}_N = \{\Lambda_{Ni}\}$, $\bar{\bar{\varepsilon}}_N = \mathrm{diag}\{\varepsilon_{Ni}\}$, i is the index of the impact points and $\mathbf{E}$ is the identity matrix. Λ_T is defined later in Sect. 4.2 as a scalar, $\mathbf{G}_{NT}$, $\mathbf{G}_{TN}$, and G_{TT} are defined according to (41) and $\bar{\bar{\boldsymbol{\mu}}} = (\mu\ \mu)$ is a vector containing the coefficients of friction. We have

$$\Lambda_{TL} = \bar{\bar{\boldsymbol{\mu}}}\boldsymbol{\Lambda}_N - \Lambda_T = 2\bar{\bar{\boldsymbol{\mu}}}\boldsymbol{\Lambda}_N - \Lambda_{TR} \tag{9}$$

Equations (7) together with the inequalities (8) represent an LCP in the classical form; i.e. a system of linear equations: $\mathbf{y} = \mathbf{A}\mathbf{x} + \mathbf{b}$, with matrices $\mathbf{A}$ and $\mathbf{b}$ known, and $\mathbf{y}$ and $\mathbf{x}$ the unknown vectors under determination, for which the following additional complementarity conditions hold: $\mathbf{y} \geq 0$, $\mathbf{x} \geq 0$, $\mathbf{y}^T\mathbf{x} = 0$. The LCP (7), (8) encapsulates a great variety of impact states such as "slip", "stick", reversal of sign and non-impulsive behavior both for single-impact and double-impact (see Sect. 4). The proposed LCP formulation (7), (8) is also readily applicable for the dynamic analysis of pounding skew bridge models, for instance, by means of an event-based methodology as in [33].

3 Contact kinematics between two planar skew rigid bodies

In addition to the inherent difficulties and uncertainties of contact phenomena in straight bridges, skew bridges present several distinct kinematical challenges as contact/impact takes place in multiple, non-predefined points, is non-centric and oblique. This section describes the contact kinematics between two adjacent skew bridge-segments. It offers equations which can be used to treat successively as many pairs of (adjacent) skew segments as necessary. As illustrated later, the same equations cover also the case of deck-abutment impact [1].

Consider two adjacent skew bridge-deck segments in plan, with skew angle α, width W, lengths L_1 and L_2, respectively, and (at rest) horizontal distance between them δ (Fig. 3). For the purposes of this analysis, each deck segment is a planar rigid body j $(j = 1, 2)$ with degrees of freedom the two horizontal translations (x_j, y_j) and the planar rotation

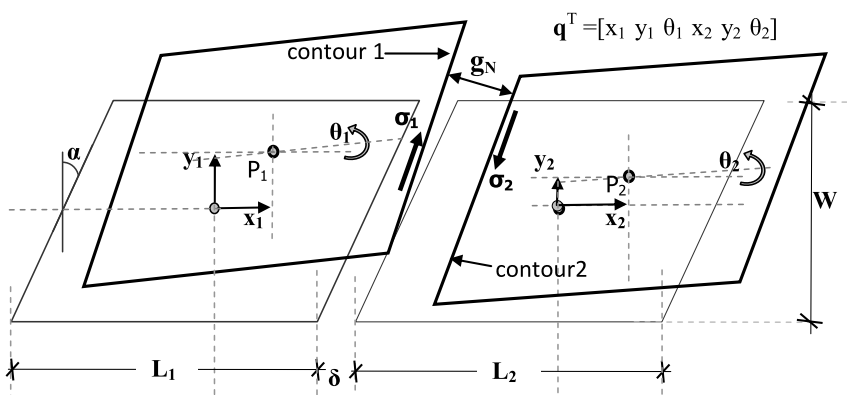

Fig. 3 Contact kinematics of two adjacent skew bridge segments for planar motion

(θ_j), all referring to an inertial frame of reference. The generalized coordinates vector of the problem is: $\mathbf{q}^T = [x_1\ y_1\ \theta_1\ x_2\ y_2\ \theta_2]$.

Points along the contours of the two bodies are determined with the help of parameters σ_j (Fig. 3). A point of contact lies between the two edges of the contour, when

$$-(W\tan\alpha)/2 \le \sigma_j \le (W\tan\alpha)/2, \quad j = 1, 2 \tag{10}$$

Hence, the position vector of a point along the contour (of the body) $j = 1, 2$ is:

$$\mathbf{r}_{P\Sigma j} = (-1)^{j+1}\begin{pmatrix} (\mathrm{c}\,\theta_j - \mathrm{s}\,\theta_j\cot\alpha)\sigma_j + \mathrm{c}\,\theta_j L_j/2 \\ (\mathrm{s}\,\theta_j + \mathrm{c}\,\theta_j\cot\alpha)\sigma_j + \mathrm{s}\,\theta_j L_j/2 \\ 0 \end{pmatrix} \quad j = 1, 2 \tag{11}$$

where the abbreviations: $\cos\theta_j \doteq \mathrm{c}\,\theta_j$ and $\sin\theta_j \doteq \mathrm{s}\,\theta_j$ are used in the same way throughout this paper; e.g. $\mathrm{c}\,\alpha = \cos\alpha$ and $\mathrm{s}\,\alpha = \sin\alpha$.

The differentiation of the position vector $\mathbf{r}_{P\Sigma j}$ with respect to σ_j, returns the normal $\mathbf{n}$ and the tangential $\mathbf{t}$ direction vectors of the two contours [29] (Fig. 3):

$$\mathbf{t}_i = (-1)^{j+1}\begin{pmatrix} \sin(\alpha-\theta_j) \\ \cos(\alpha-\theta_j) \\ 0 \end{pmatrix}, \qquad \mathbf{n}_j = (-1)^{j}\begin{pmatrix} \cos(\alpha-\theta_j) \\ -\sin(\alpha-\theta_j) \\ 0 \end{pmatrix}, \quad j = 1, 2 \tag{12}$$

The distance vector $\mathbf{r}_D$, as a function of parameters σ_j (e.g. Fig. 4) is

$$\mathbf{r}_D = \begin{pmatrix} (1-\mathrm{c}\,\theta_2)L_2/2 + (1-\mathrm{c}\,\theta_1)L_1/2 + \delta + x_2 - x_1 - (\mathrm{c}\,\theta_2 - \mathrm{s}\,\theta_2\cot\alpha)\sigma_2 - (\mathrm{c}\,\theta_1 - \mathrm{s}\,\theta_1\cot\alpha)\sigma_1 \\ -\mathrm{s}\,\theta_2 L_2/2 - \mathrm{s}\,\theta_1 L_1/2 + y_2 - y_1 - (\mathrm{s}\,\theta_2 + \mathrm{c}\,\theta_2\cot\alpha)\sigma_2 - (\mathrm{s}\,\theta_1 + \mathrm{c}\,\theta_1\cot\alpha)\sigma_1 \\ 0 \end{pmatrix} \tag{13}$$

3.1 Relative distance in the normal direction of contact

Contact between two adjacent skew bridge deck-segments can take place either at an edge, single-point contact (Fig. 4), or along a side—full edge (multi-point contact (Fig. 5). Single-point contact appears between any of the two edges of one body/contour and at an unknown contour point of the adjacent body. Two cases are distinguished (Fig. 4):

Case 1: One of the two edges of contour 2 comes in contact with an unknown point of contour 1 (Fig. 4 top). The condition $\mathbf{r}_D^T\mathbf{t}_1 = 0$ (14):

$$\begin{aligned} \mathbf{r}_D^T\mathbf{t}_1 = 0 \quad \Rightarrow \\ \frac{\sigma_1}{\mathrm{s}\,\alpha} = &-\mathrm{s}\,\alpha L_1/2 + \big[(1-\mathrm{c}\,\theta_2)L_2/2 + L_1/2 + \delta \\ &+ x_2 - x_1\big]\sin(\alpha-\theta_1) + (-\mathrm{s}\,\theta_2 L_2/2 \\ &+ y_2 - y_1)\cos(\alpha-\theta_1) \\ &- \cos(\theta_1-\theta_2)\frac{\sigma_2}{\mathrm{s}\,\alpha} \end{aligned} \tag{14}$$

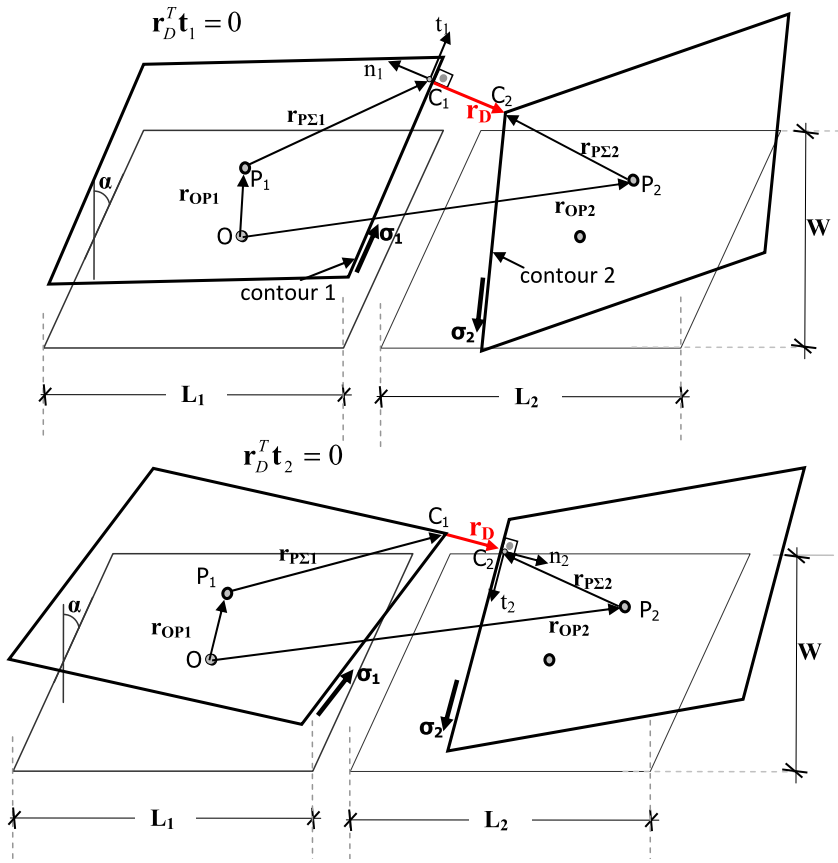

Fig. 4 Point contact between two planar skew rigid bodies. Case 1 ($g_N = -\mathbf{r}_D^T\mathbf{n}_1$) (*top*), Case 2 ($g_N = \mathbf{r}_D^T\mathbf{n}_2$) (*bottom*)

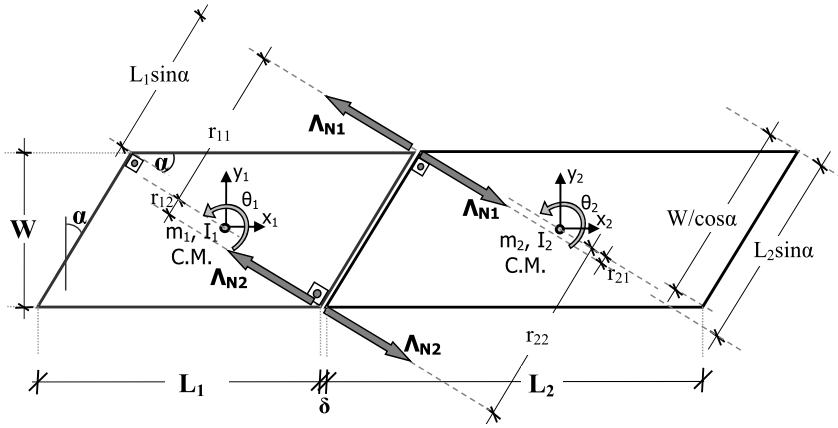

Fig. 5 Full-edge frictionless impact between two skew deck segments (considered as rigid bodies)

determines the point of contact on contour 1 (parameter σ_1) which, in addition, has to satisfy the constraint (10).

The inner product of the distance vector $\mathbf{r}_D$ with the orthonormal vector $\mathbf{n}_1$ (Fig. 4 top) yields the pertinent relative distance in the normal direction g_N between the two adjacent rigid bodies [29]:

$$\begin{aligned} g_N &= -\mathbf{r}_D^T\mathbf{n}_1 \\ &= \big[(1-\mathrm{c}\,\theta_2)L_2/2 + (1-\mathrm{c}\,\theta_1)L_1/2 + \delta + x_2 \\ &\quad - x_1\big]\cos(\alpha-\theta_1) + (-\mathrm{s}\,\theta_2 L_2/2 - \mathrm{s}\,\theta_1 L_1/2 \\ &\quad + y_2 - y_1)\sin(\theta_1-\alpha) \\ &\quad - \sin(\theta_1-\theta_2)\frac{\sigma_2}{\mathrm{s}\,\alpha} \end{aligned} \tag{15}$$

Case 2: One of the edges of contour 1 comes in contact with an unknown point of contour 2 (Fig. 4 bottom). Similarly to Case 1, we have

$$\begin{aligned}\mathbf{r}_D^T\mathbf{t}_2 = 0 \quad \Rightarrow \\ \frac{\sigma_2}{\mathrm{s}\,a} = &-\mathrm{s}\,\alpha L_2/2 + (-\mathrm{s}\,\theta_1 L_1/2 + y_2 - y_1) \\ &\times \cos(\alpha-\theta_2) - \cos(\theta_1-\theta_2)\frac{\sigma_1}{\mathrm{s}\,a} \\ &+ \left[(1-\mathrm{c}\,\theta_1)L_1/2 + L_2/2 + \delta + x_2 - x_1\right] \\ &\times \sin(\alpha-\theta_2) \end{aligned} \tag{16}$$

And:

$$\begin{aligned} g_N &= \mathbf{r}_D^T\mathbf{n}_2 \\ &= \left[(1-\mathrm{c}\,\theta_2)L_2/2 + (1-\mathrm{c}\,\theta_1)L_1/2 + \delta \right. \\ &\quad \left. + x_2 - x_1\right]\cos(\alpha-\theta_2) + (-\mathrm{s}\,\theta_2 L_2/2 \\ &\quad - \mathrm{s}\,\theta_1 L_1/2 + y_2 - y_1)\sin(\theta_2-\alpha) \\ &\quad + \sin(\theta_1-\theta_2)\frac{\sigma_1}{\mathrm{s}\,\alpha} \end{aligned} \tag{17}$$

Equation (17) verifies the pertinent equations of the simpler (deck-abutment) impact case [1], if the body "2" is replaced with a rigid boundary: i.e. $x_2 = y_2 = \theta_2 = 0$. In summary, when $\theta_1 \neq \theta_2$ (Fig. 4) the distance is determined by the minimum distance yielded from (15) and (17), which does not violate the constraint (10).

3.2 Contact velocities

The differentiation of the pertinent relative distances, with respect to time, gives the contact velocities in the normal direction. In the tangential direction, contact velocities are determined with the help of the corresponding tangential direction vectors $\mathbf{t}$ and the Jacobean matrices $\mathbf{J}_{Cj}$ [29]. The same two cases hold.

Case 1 ($g_N = -\mathbf{r}_D^T\mathbf{n}_1$): For the normal contact velocity γ_N the differentiation of (15) gives

$$\gamma_N = \mathbf{w}_N^T\mathbf{u}$$

$$\mathbf{w}_N = \begin{pmatrix} -\cos(\alpha-\theta_1) \\ \sin(\alpha-\theta_1) \\ \tilde{r}_{N1} \\ \cos(\alpha-\theta_1) \\ -\sin(\alpha-\theta_1) \\ \tilde{r}_{N2} \end{pmatrix}$$

$$\begin{aligned} \tilde{r}_{N1} = \Big\{ &(-\mathrm{s}\,\theta_2 L_2/2 + y_2 - y_1)\cos(\alpha-\theta_1) \\ &- \frac{\sigma_2}{\mathrm{s}\,\alpha}\cos(\theta_1-\theta_2) + \left[(1-\mathrm{c}\,\theta_2)L_2/2 \right. \\ &\left. + L_1/2 + \delta + x_2 - x_1\right]\sin(\alpha-\theta_1)\Big\} \\ \tilde{r}_{N2} = \Big\{ &\sin(\alpha-\theta_1+\theta_2)L_2/2 + \frac{\sigma_2}{\mathrm{s}\,\alpha}\cos(\theta_1-\theta_2)\Big\} \end{aligned} \tag{18}$$

For the tangential contact velocity γ_T we have

$$\gamma_T = \mathbf{w}_T^T\mathbf{u}$$

$$\mathbf{w}_T = \mathbf{t}_1^T(\mathbf{J}_{C1} - \mathbf{J}_{C2}) = \begin{pmatrix} \sin(\alpha-\theta_1) \\ \cos(\alpha-\theta_1) \\ \tilde{r}_{T1} \\ -\sin(\alpha-\theta_1) \\ -\cos(\alpha-\theta_1) \\ \tilde{r}_{T2} \end{pmatrix}$$

$$\begin{aligned} \tilde{r}_{T1} &= \mathrm{c}\,\alpha L_1/2 \\ \tilde{r}_{T2} &= \Big\{\cos(\alpha+\theta_2-\theta_1)L_2/2 - \sin(\theta_2-\theta_1) \\ &\quad \times \frac{\sigma_2}{\sin\alpha}\Big\} \end{aligned} \tag{19}$$

Case 2 ($g_N = \mathbf{r}_D^T\mathbf{n}_2$): Similarly, with Case 1 we obtain

$$\gamma_N = \mathbf{w}_N^T\mathbf{u}$$

$$\mathbf{w}_N = \begin{pmatrix} -\cos(\alpha-\theta_2) \\ \sin(\alpha-\theta_2) \\ \tilde{r}_{N1} \\ \cos(\alpha-\theta_2) \\ -\sin(\alpha-\theta_2) \\ \tilde{r}_{N2} \end{pmatrix}$$

$$\begin{aligned} \tilde{r}_{N1} &= \Big\{\sin(\alpha+\theta_1-\theta_2)L_1/2 + \frac{\sigma_1}{\mathrm{s}\,\alpha}\cos(\theta_1-\theta_2)\Big\} \\ \tilde{r}_{N2} &= \Big\{\left[L_2/2 + (1-\mathrm{c}\,\theta_1)L_1/2 + \delta + x_2 - x_1\right] \\ &\quad \times \sin(\alpha-\theta_2) + (-\mathrm{s}\,\theta_1 L_1/2 + y_2 - y_1) \\ &\quad \times \cos(\alpha-\theta_2) - \frac{\sigma_1}{\mathrm{s}\,\alpha}\cos(\theta_1-\theta_2)\Big\} \end{aligned} \tag{20}$$

And:

$$\gamma_T = \mathbf{w}_T^T\mathbf{u}$$

$$\mathbf{w}_T = \begin{pmatrix} \sin(\alpha-\theta_2) \\ \cos(\alpha-\theta_2) \\ \tilde{r}_{T1} \\ -\sin(\alpha-\theta_2) \\ -\cos(\alpha-\theta_2) \\ \tilde{r}_{T2} \end{pmatrix}$$

$$\tilde{r}_{T1} = \left\{ \cos(\alpha + \theta_1 - \theta_2) L_1/2 - \sin(\theta_1 - \theta_2) \frac{\sigma_1}{\mathrm{s}\alpha} \right\}$$
$$\tilde{r}_{T2} = \mathrm{c}\alpha L_2/2 \tag{21}$$

4 Nonsmooth analysis

4.1 Double frictionless impact

Utilizing the rigid body assumption, full-edge impact is modeled as a double-point impact and the discussion starts with the frictionless case. Full-edge contact (Fig. 5) occurs when the two bodies come to contact while their normal and tangential direction vectors are parallel to each other (i.e. $\mathbf{n}_1^T \mathbf{t}_2 = 0$ or equivalently $\mathbf{n}_2^T \mathbf{t}_1 = 0$). Indeed, the kinematical conditions $\mathbf{n}_1^T \mathbf{t}_2 = 0$ or $\mathbf{n}_2^T \mathbf{t}_1 = 0$ confirm that full-edge impact occurs when the pre-impact rotations are equal $\theta_1^- = \theta_2^-$:

$$\mathbf{n}_1^T \mathbf{t}_2 = 0 \quad \Rightarrow \quad \sin(\theta_1 - \theta_2) = 0 \tag{22}$$

In this case the relative contact distance is given from either (15) or (17). Without loss of generality, it is assumed that the pre-impact rotations are both equal to zero $\theta_1^- = \theta_2^- = 0$, while the pre-impact translational velocities arbitrary. Equations (15) and (17) simplify to

$$g_N = -\mathbf{r}_D^T \mathbf{n}_1 = \mathbf{r}_D^T \mathbf{n}_2$$
$$= (\delta + x_2 - x_1)\,\mathrm{c}\alpha + (y_2 - y_1)\,\mathrm{s}\alpha = 0 \tag{23}$$

For $\theta_1^- = \theta_2^- = 0$, (18) and (20) give the same normal contact velocity. Similarly, (19) and (21) return the same tangential contact velocity. The direction vector $\mathbf{W}_N$, simplifies to:

$$\mathbf{w}_{N1}^T = \left(-\mathrm{c}\alpha \quad \mathrm{s}\alpha \quad \overbrace{\left(\frac{\mathrm{s}\alpha L_1}{2} + \frac{W}{2\mathrm{c}\alpha}\right)}^{r_{11}} \quad \mathrm{c}\alpha \quad -\mathrm{s}\alpha \quad \underbrace{\left(\frac{\mathrm{s}\alpha L_2}{2} - \frac{W}{2\mathrm{c}\alpha}\right)}_{r_{21}} \right)$$
$$\mathbf{w}_{N2}^T = \left(-\mathrm{c}\alpha \quad \mathrm{s}\alpha \quad \overbrace{\left(\frac{\mathrm{s}\alpha L_1}{2} - \frac{W}{2\mathrm{c}\alpha}\right)}^{r_{12}} \quad \mathrm{c}\alpha \quad -\mathrm{s}\alpha \quad \underbrace{\left(\frac{\mathrm{s}\alpha L_2}{2} + \frac{W}{2\mathrm{c}\alpha}\right)}_{r_{22}} \right) \tag{24}$$
$$\mathbf{W}_N^T = \begin{pmatrix} \mathbf{w}_{N1}^T \\ \mathbf{w}_{N2}^T \end{pmatrix}$$

where r_{11}, r_{12}, r_{21} and r_{22} are the lever arms shown in Fig. 5. Hence, the $\mathbf{G}_{NN}$ matrix becomes

$$\mathbf{G}_{NN} = \begin{pmatrix} \frac{1}{m_1} + \frac{1}{m_2} + \frac{r_{11}^2}{I_1} + \frac{r_{21}^2}{I_2} & \frac{1}{m_1} + \frac{1}{m_2} + \frac{r_{11} r_{12}}{I_1} + \frac{r_{21} r_{22}}{I_2} \\ \frac{1}{m_1} + \frac{1}{m_2} + \frac{r_{11} r_{12}}{I_1} + \frac{r_{21} r_{22}}{I_2} & \frac{1}{m_1} + \frac{1}{m_2} + \frac{r_{12}^2}{I_1} + \frac{r_{22}^2}{I_2} \end{pmatrix} \tag{25}$$

The inverse of the matrix $\mathbf{G}_{NN}$, $\mathbf{G}_{NN}^{-1}$, is the effective mass during collision in the normal direction [29]:

$$\mathbf{G}_{NN}^{-1} = \frac{1}{|\mathbf{G}_{NN}|} \begin{pmatrix} \frac{1}{m_1} + \frac{1}{m_2} + \frac{r_{12}^2}{I_1} + \frac{r_{22}^2}{I_2} & -\left(\frac{1}{m_1} + \frac{1}{m_2} + \frac{r_{11} r_{12}}{I_1} + \frac{r_{21} r_{22}}{I_2}\right) \\ -\left(\frac{1}{m_1} + \frac{1}{m_2} + \frac{r_{11} r_{12}}{I_1} + \frac{r_{21} r_{22}}{I_2}\right) & \frac{1}{m_1} + \frac{1}{m_2} + \frac{r_{11}^2}{I_1} + \frac{r_{21}^2}{I_2} \end{pmatrix} \tag{26}$$

in which the determinant $|\mathbf{G}_{NN}|$ is given in the Appendix.

$$|\mathbf{G}_{NN}| = \frac{(r_{11} r_{21} - r_{12} r_{22})^2}{I_1 I_2} + \left[\frac{(r_{11} - r_{12})^2}{I_1} + \frac{(r_{21} - r_{22})^2}{I_2} \right] \left(\frac{1}{m_1} + \frac{1}{m_2} \right) \tag{27}$$

According to Newton's impact law [29], the vector of impulses $\boldsymbol{\Lambda}_N$ along the normal direction of contact is:

$$\boldsymbol{\Lambda}_N = \begin{pmatrix} \Lambda_{N1} \\ \Lambda_{N2} \end{pmatrix} = -\mathbf{G}_{NN}^{-1} (\mathbf{E} + \bar{\bar{\boldsymbol{\varepsilon}}}_N) \boldsymbol{\gamma}_N^- \tag{28}$$

where $\mathbf{E}$, is the identity matrix. When the coefficients of restitution at the two impacts are the same and equal

with ε_N, (28) simplifies to

$$\begin{aligned}
&\Lambda_{N1}\frac{|\mathbf{G}_{NN}|}{\gamma_N^-}\\
&\quad=-(1+\varepsilon_N)\left(r_{12}\frac{r_{12}-r_{11}}{I_1}+r_{22}\frac{r_{22}-r_{21}}{I_2}\right)\\
&\quad=-\left(1+\varepsilon_N\right)\frac{W}{\mathrm{c}\,\alpha}\left(\frac{r_{22}}{I_2}-\frac{r_{12}}{I_1}\right)\\
&\Lambda_{N2}\frac{|\mathbf{G}_{NN}|}{\gamma_N^-}\\
&\quad=-\left(1+\varepsilon_N\right)\left(r_{11}\frac{r_{11}-r_{12}}{I_1}+r_{21}\frac{r_{21}-r_{22}}{I_2}\right)\\
&\quad=-(1+\varepsilon_N)\frac{W}{\mathrm{c}\,\alpha}\left(\frac{r_{11}}{I_1}-\frac{r_{21}}{I_2}\right)
\end{aligned}\tag{29}$$

In this case, the post-impact angular velocities of the two bodies are (4) equal and both positive (in the direction of increasing the skew angle):

$$\begin{aligned}
&u_{\theta 1}^{+}=u_{\theta 2}^{+}\\
&\quad=-\frac{(1+\varepsilon_N)\gamma_N^-}{|\mathbf{G}_{NN}|I_1I_2}\frac{L_1+L_2}{2}\frac{W^2\sin\alpha}{\cos^2\alpha}>0
\end{aligned}\tag{30}$$

Equations (29) give the normal impulses Λ_{N1} and Λ_{N2} as a function of the geometry (α, L_1, L_2, W), the coefficient of restitution (in the normal direction) ε_N, and the inertia parameters (the mass moments of inertia I_1, I_2 and the determinate $|\mathbf{G}_{NN}|$). In addition, the physical inequality constraint $\boldsymbol{\Lambda}_N\geq 0$ should hold, to ensure the unilateral nature of (dry) impact. In multi-point impacts the satisfaction of the inequality constraint demands special attention [29]. Taking into account that by definition: $(1+\varepsilon_N)>0$, $|\mathbf{G}_{NN}|>0$ and that contact occurs only when the relative velocity is negative $\gamma_N^-\leq 0$ (which denotes approach), we have

$$\begin{aligned}
&\Lambda_{N1}>0 \quad\Rightarrow\quad \frac{I_1}{I_2}>\frac{\eta_1-1}{\eta_2+1}\\
&\Lambda_{N2}>0 \quad\Rightarrow\quad \frac{I_2}{I_1}>\frac{\eta_2-1}{\eta_1+1}
\end{aligned}\tag{31}$$

where η_j is the dimensionless skew ratio introduced, for frictionless impact, in Dimitrakopoulos [1]:

$$\eta_j=\frac{\sin 2\alpha}{2(W/L_j)},\quad j=1,2\tag{32}$$

η_j relates the ratio of the two sides in plan (L, W) with the skew angle, α. Inequalities (31) unveil a mechanism considerably more complicated compared with the case of a skew rigid body pounding against an inelastic half-space [1]. In particular, the signs of the impulses depend not only on the geometry (and hence the proposed dimensionless criteria η_1, η_2), but also on the ratio of the mass moments of inertial of the two bodies I_1/I_2. The following special cases shed some light on the underlying mechanism of the examined impact problem.

1. When the two segments are of equal length $L_1=L_2\rightarrow\eta_1/\eta_2=I_1/I_2=1$, the normal impulses in both points are always positive, since

$$\begin{aligned}
&\Lambda_{N1}>0 \quad\Rightarrow\quad \frac{I_1}{I_2}>\frac{\eta_1-1}{\eta_2-1}\\
&\quad\Rightarrow\quad 1>\frac{\eta-1}{\eta+1}\quad\Rightarrow\quad 1>-1\\
&\Lambda_{N2}>0 \quad\Rightarrow\quad \frac{I_2}{I_1}>\frac{\eta_2-1}{\eta_1+1}\\
&\quad\Rightarrow\quad 1>\frac{\eta-1}{\eta+1}\quad\Rightarrow\quad 1>-1
\end{aligned}\tag{33}$$

2. When the two segments have different lengths but equal inertias, we have

$$\begin{aligned}
&\Lambda_{N1}>0 \quad\Rightarrow\quad r_{22}>r_{12}\quad\Rightarrow\quad \eta_1-\eta_2<2\\
&\quad\Rightarrow\quad (L_1-L_2)<\frac{4W}{\sin 2\alpha}\\
&\Lambda_{N2}>0 \quad\Rightarrow\quad r_{11}>r_{21}\quad\Rightarrow\quad \eta_2-\eta_1<2\\
&\quad\Rightarrow\quad (L_2-L_1)<\frac{4W}{\sin 2\alpha}
\end{aligned}\tag{34}$$

   In practice, the length of the segment is directly related to its mass, however, this theoretical assumption reveals the effect of the geometry on the outcome of the impact. Figure 6 visualizes an example where $\Lambda_{N2}=0$ ($r_{11}=r_{21}$).

3. When the inertia of one segment is infinite compared to that of the other segment, e.g. $I_2/I_1\rightarrow\infty$, we have

$$\begin{aligned}
&\Lambda_{N1}\frac{I_1|\mathbf{G}_{NN}|}{\gamma_N^-}=(1+\varepsilon_N)\frac{W}{\mathrm{c}\,\alpha}r_{12}\quad\Rightarrow\quad \Lambda_{N1}>0\\
&\quad\Rightarrow\quad r_{12}<0\quad\Rightarrow\quad \eta_1<1\\
&\Lambda_{N2}\frac{I_1|\mathbf{G}_{NN}|}{\gamma_N^-}=(1+\varepsilon_N)\frac{W}{\mathrm{c}\,\alpha}r_{11}\quad\Rightarrow\quad \Lambda_{N2}>0\\
&\quad\Rightarrow\quad r_{11}>0\quad\Rightarrow\quad \eta_1>-1
\end{aligned}\tag{35}$$

   According to (35), when $\eta_1>1$ impulse at the acute corner becomes negative $\Lambda_{N1}<0$ which is not feasible. The physical interpretation of a negative impulse is that contact at that point is lost and

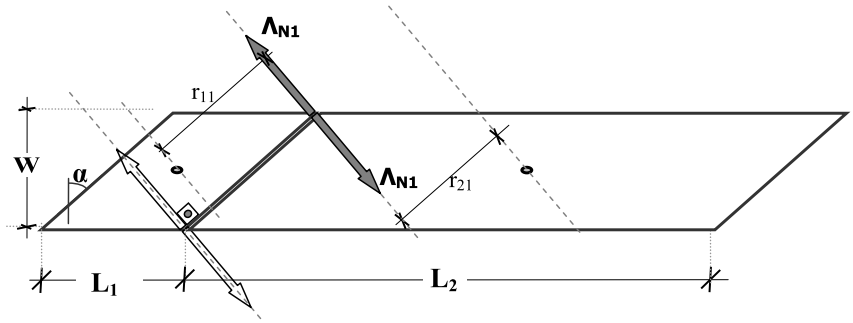

Fig. 6 Assuming the masses and mass moments of inertia of the two bodies are equal, contact at point 2 is lost (*white arrows*) when $r_{11} = r_{21}$

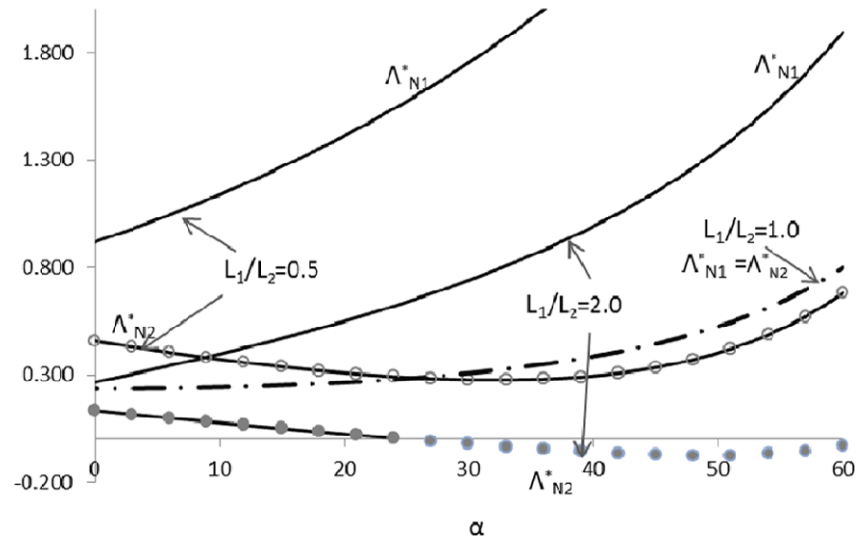

Fig. 7 The results of (37). The negative sign of impulse at contact point 2 indicates that contact at that point is lost

hence the formulation of the impact as double impact does not hold. Instead, when $\eta_1 > 1$, the impact problem should be treated as a single impact at the obtuse corner at which the impulse is positive, $\Lambda_{N2} > 0$. In short, the behavior for $I_2/I_1 \to \infty$ (or $I_1/I_2 \to \infty$) corresponds to the simpler case of a single skew segment pounding against an inelastic half-space [1].

4. To further investigate the impact mechanism, the mass of the substructure is assumed negligible compared with the mass of the deck segments. Thus, the mass moments of inertia of the two bridge segments are given solely by the inertia of the corresponding skew deck segments (rigid bodies):

$$I_i = m_i\left[\frac{L_i^2}{12} + \frac{W^2}{12\cos^2 a}\right], \quad i = 1, 2 \tag{36}$$

With the help of (36), and the additional assumption that the two skew deck segments have the same density hence the masses ratio is equal with the lengths ratio, $m_1/m_2 = L_1/L_2$ (29) gives

$$\begin{aligned}\Lambda^*_{N1} &= \Lambda_{N1}\frac{m_1|\mathbf{G}_{NN}|}{-3\gamma_N^-(1+\varepsilon_N)} \\ &= \frac{L_1}{L_2}\frac{\frac{L_2}{W}\sin 2\alpha + 2}{(\frac{L_2}{W}\cos\alpha)^2 + 1} - \frac{\frac{L_1}{W}\sin 2\alpha - 2}{(\frac{L_1}{W}\cos\alpha)^2 + 1} \\ \Lambda^*_{N2} &= \Lambda_{N2}\frac{m_2|\mathbf{G}_{NN}|}{-3\gamma_N^-(1+\varepsilon_N)} \\ &= \frac{L_2}{L_1}\frac{\frac{L_1}{W}\sin 2\alpha + 2}{(\frac{L_1}{W}\cos\alpha)^2 + 1} - \frac{\frac{L_2}{W}\sin 2\alpha - 2}{(\frac{L_2}{W}\cos\alpha)^2 + 1}\end{aligned} \tag{37}$$

where $\Lambda^*_{N1}, \Lambda^*_{N2}$ are normalized values of Λ_{N1} and Λ_{N2} respectively. Figure 7 presents the impulses Λ^*_{N1} and Λ^*_{N2} for different skew angles and length ratios. Most importantly, Fig. 7 demonstrates that when the length ratio assumes high values, (e.g. $L_1/L_2 = 2.0$) contact at one of the two contact points may be lost (in this case at point 2)

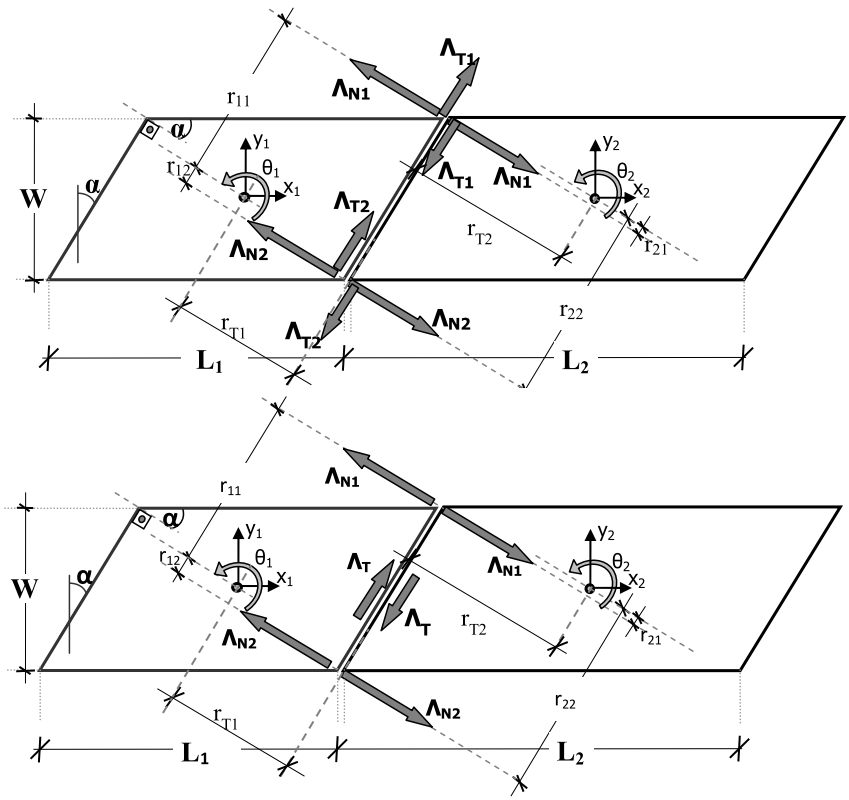

Fig. 8 Full-edge frictional impact between two skew deck segments (considered as rigid bodies). Conventional (*top*) and proposed (*bottom*) simulation approach

for a sufficient high value of the skew angle (α). In other words, even full edge impact may in essence be a single point impact, depending on the inertia of the two segments and the whole geometry (in plan). This non-intuitive impact behavior has not received the attention it deserves when simulating the seismic behavior of skew bridges with in-deck joints.

4.2 Double frictional impact

Consider the frictional case of the full-edge impact of Fig. 8. The "conventional" simulation approach (Fig. 8 top) is to consider the normal and the tangential $\boldsymbol{\Lambda}_T = \{\Lambda_{Ti}\}$ impulses of each contact point i explicitly (Fig. 8 top). In this case the direction matrix of the tangential contact impulses is

$$\mathbf{W}_T^T = \begin{pmatrix} s\alpha & \mathrm{c}\,\alpha & r_{T1} & -s\alpha & -\mathrm{c}\,\alpha & r_{T2} \\ s\alpha & \mathrm{c}\,\alpha & r_{T1} & -s\alpha & -\mathrm{c}\,\alpha & r_{T2} \end{pmatrix}$$
$$\mathbf{W}_T \in \mathbb{R}^{6\times 2} \tag{38}$$

This description (Fig. 8 top) of double impact, neglects that the two (point) impacts are linearly dependent in the tangential direction and, as a consequence $\mathbf{G}_{NT}$, $\mathbf{G}_{TN}$ and $\mathbf{G}_{TT}$ (6) are all singular matrices. This is a typical case of *overconstrained* impacts which arise often in multibody dynamics with multicontacts [26]. The present study proposes an alternative description of the double impact, which does not over-constrain the problem and, at the same time, allows for a closed-form solution avoiding all singularities during solution of the LCP. Instead of examining the tangential impulse in each point explicitly (Fig. 8 top), the proposed simulation considers solely the resultant tangential impulse Λ_T (Fig. 8 top). With reference to Fig. 8, the following straightforward relationship holds:

$$\Lambda_{T1} + \Lambda_{T2} = \mu\Lambda_{N1} + \mu\Lambda_{N2} = \begin{pmatrix} \mu & \mu \end{pmatrix} \begin{pmatrix} \Lambda_{N1} \\ \Lambda_{N2} \end{pmatrix}$$
$$= \bar{\bar{\boldsymbol{\mu}}}\boldsymbol{\Lambda}_N = \Lambda_T \tag{39}$$

where $\bar{\bar{\boldsymbol{\mu}}} = \begin{pmatrix} \mu & \mu \end{pmatrix}$ (Fig. 8 bottom). Compared with the ad hoc approach, proposed in [1], specifically for double stick, the present proposal is more generic as it is valid for all feasible impact states (Fig. 9). The di-

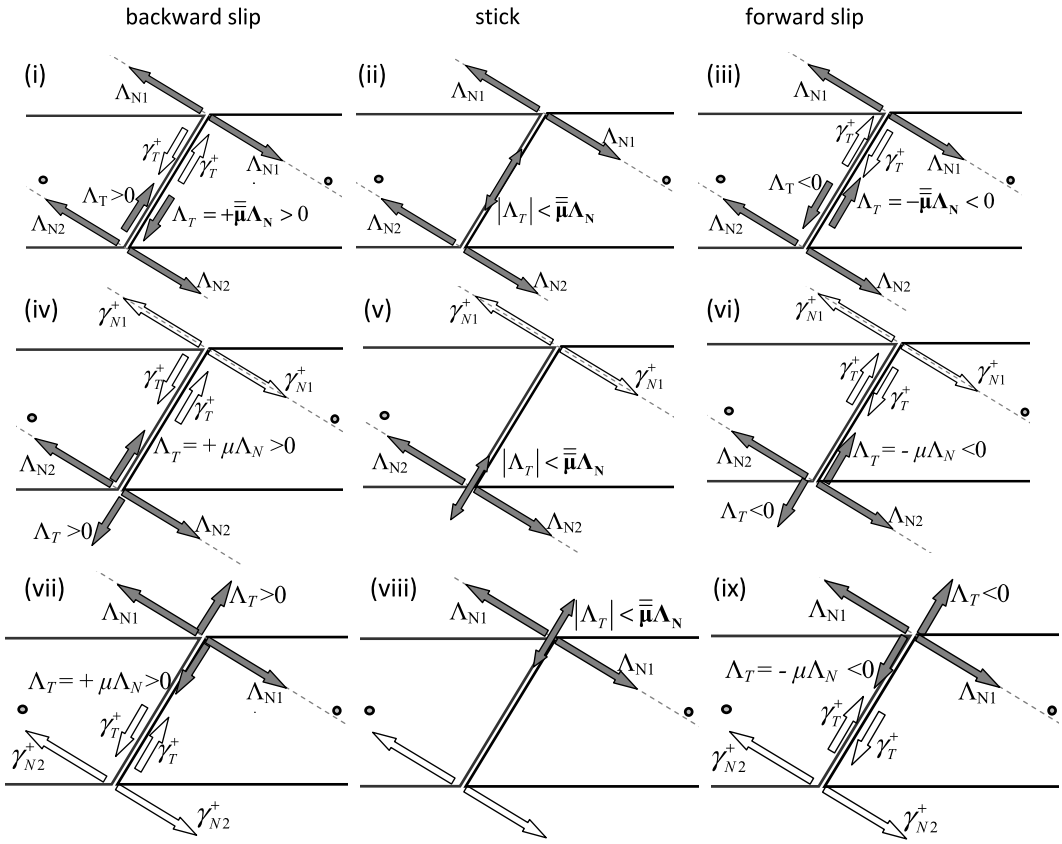

Fig. 9 The potential impact states (solutions) of the double-impact problem of Fig. 8

rection vector for the single tangential impulse (Fig. 8 bottom) becomes

$$\mathbf{W}_T^T = \begin{pmatrix} s\alpha & c\alpha & r_{T1} & -s\alpha & -c\alpha & r_{T2} \end{pmatrix} \quad \mathbf{W}_T \in \mathbb{R}^{6\times 1} \tag{40}$$

The description of the normal impulses remains the same (24). Then, $\mathbf{G}_{NT}$, $\mathbf{G}_{TN}$, and G_{TT} are, see (6),

$$\mathbf{G}_{NT} = \mathbf{W}_N^T \mathbf{M}^{-1} \mathbf{W}_T = \begin{pmatrix} \frac{r_{11}r_{T1}}{I_1} + \frac{r_{21}r_{T2}}{I_2} \\ \frac{r_{12}r_{T1}}{I_1} + \frac{r_{22}r_{T2}}{I_2} \end{pmatrix} = \mathbf{G}_{TN}^T \quad \mathbf{G}_{NT} \in \mathbb{R}^{2\times 1}$$
$$G_{TT} = \mathbf{W}_T^T \mathbf{M}^{-1} \mathbf{W}_T = \frac{1}{m_1} + \frac{1}{m_2} + \frac{r_{T1}^2}{I_1} + \frac{r_{T2}^2}{I_2} \quad G_{TT} \in \mathbb{R}^{1\times 1} \tag{41}$$

The discussion of each potential impact state follows closely the analysis of the simpler impact configuration presented in [1]. The potential outcomes of the frictional impact of Fig. 8 are (Fig. 9): three (3) impact states wherein both impact points are active ($\Lambda_{N1} > 0$ and $\Lambda_{N2} > 0$) (double forward slip, double backward slip and double stick), and the six impact states, wherein only one of the two impact points presents a positive impulse ($\Lambda_{N1} > 0$ or $\Lambda_{N2} > 0$). Double impacts where $\Lambda_N = 0$ holds at both impact points, lack physical interpretation and are not considered.

Double backward slip (Fig. 9(i)) The complementarity conditions (8) for $\Lambda_{N1} > 0$, $\Lambda_{N2} > 0$ and $\Lambda_T = \mu(\Lambda_{N1} + \Lambda_{N2}) = +\bar{\bar{\boldsymbol{\mu}}}\boldsymbol{\Lambda}_N$ yield $v_{N1} = v_{N2} = v_{TR} = 0$, $\Lambda_{TR} = 2\bar{\bar{\boldsymbol{\mu}}}\boldsymbol{\Lambda}_N$ and $\Lambda_{TL} = 0$. It follows from (7) that the impulses in the normal direction are

$$\boldsymbol{\Lambda}_N = -(\mathbf{G}_{NN} + \mathbf{G}_{NT}\bar{\bar{\boldsymbol{\mu}}})^{-1}(\bar{\bar{\varepsilon}}_N + \mathbf{E})\boldsymbol{\gamma}_N^- \quad \Rightarrow$$
$$\begin{pmatrix} \Lambda_{N1} \\ \Lambda_{N2} \end{pmatrix} = -\frac{(1+\varepsilon_N)\gamma_N^-}{D_1} \times \begin{pmatrix} \frac{(r_{12}-r_{11})(r_{12}+\mu r_{T1})}{I_1} + \frac{(r_{22}-r_{21})(r_{22}+\mu r_{T2})}{I_2} \\ \frac{(r_{11}-r_{12})(r_{11}+\mu r_{T1})}{I_1} + \frac{(r_{21}-r_{22})(r_{21}+\mu r_{T2})}{I_2} \end{pmatrix} \tag{42}$$

The determinate $D_1 = |\mathbf{G}_{NN} + \mathbf{G}_{NT}\bar{\bar{\mu}}|$ and matrix $(\mathbf{G}_{NN} + \mathbf{G}_{NT}\bar{\bar{\mu}})^{-1}$ are given in the Appendix. With the help of (42), the tangential post-impact velocity, from (7), becomes

$$\begin{aligned}\frac{\gamma_T^+}{\gamma_N^-} &= \frac{\gamma_T^-}{\gamma_N^-} \\ &- \frac{1+\varepsilon_N}{D_1}\left\{\frac{\mu}{\bar{m}}\left[\frac{(r_{11}-r_{12})^2}{I_1}+\frac{(r_{21}-r_{22})^2}{I_2}\right]\right. \\ &+ \frac{1}{I_1 I_2}\left[(r_{21}-r_{22})r_{T1}+(r_{12}-r_{11})r_{T2}\right] \\ &\times\left[(r_{21}-r_{22})\mu r_{T1}+(r_{12}-r_{11})\mu r_{T2}+r_{12}r_{21}\right. \\ &\left.\left.- r_{11}r_{22}\right]\right\} \end{aligned} \tag{43}$$

In the case of double backward slip, the post-impact angular velocities of the two bodies are equal, since (4) gives

$$\begin{aligned}u_{\theta 1}^+ = u_{\theta 2}^+ &= -(1+\varepsilon_N)\frac{\gamma_N^-}{D_1}\frac{1}{I_1 I_2}\frac{L_1+L_2}{2} \\ &\times \frac{W^2}{\cos\alpha}(\tan\alpha+\mu) > 0 \end{aligned} \tag{44}$$

Double forward slip (Fig. 9(iii)) The analysis of the double forward slip case (Fig. 9(iii)) follows the same procedure as for double backward slip. The impulses in the normal direction are

$$\begin{aligned}&\boldsymbol{\Lambda}_N = -(1+\varepsilon_N)\gamma_N^-(\mathbf{G}_{NN}-\mathbf{G}_{NT}\bar{\bar{\mu}})^{-1}\begin{pmatrix}1\\1\end{pmatrix} \quad \Rightarrow \\ &\begin{pmatrix}\Lambda_{N1}\\ \Lambda_{N2}\end{pmatrix} \\ &= -(1+\varepsilon_N)\frac{\gamma_N^-}{D_2} \\ &\times\begin{pmatrix}-\frac{(r_{11}-r_{12})(r_{12}-\mu r_{T1})}{I_1}-\frac{(r_{21}-r_{22})(r_{22}-\mu r_{T2})}{I_2}\\ \frac{(r_{11}-r_{12})(r_{11}-\mu r_{T1})}{I_1}+\frac{(r_{21}-r_{22})(r_{21}-\mu r_{T2})}{I_2}\end{pmatrix} \end{aligned} \tag{45}$$

Again, the determinate $D_2 = |\mathbf{G}_{NN} - \mathbf{G}_{NT}\bar{\bar{\mu}}|$ and matrix $(\mathbf{G}_{NN} - \mathbf{G}_{NT}\bar{\bar{\mu}})^{-1}$ are given in the Appendix. The pertinent tangential post-impact velocity is

$$\begin{aligned}\frac{\gamma_T^+}{\gamma_N^-} &= \frac{\gamma_T^-}{\gamma_N^-} - (1+\varepsilon_N) \\ &\times \frac{1}{D_2}\left\{\frac{\mu}{\bar{m}}\left[\frac{(r_{11}-r_{12})^2}{I_1}+\frac{(r_{21}-r_{22})^2}{I_2}\right]\right. \\ &+ \frac{1}{I_1 I_2}\left[(r_{21}-r_{22})r_{T1}+(r_{12}-r_{11})r_{T2}\right] \\ &\times\left[(r_{21}-r_{22})\mu r_{T1}+(r_{12}-r_{11})\mu r_{T2}\right. \\ &\left.\left.+ r_{11}r_{22}-r_{21}r_{12}\right]\right\} \end{aligned} \tag{46}$$

Double stick (Fig. 9(ii)) Double stick takes place when $\Lambda_{N1} > 0$, $\Lambda_{N2} > 0$ and $|\Lambda_T| < \mu(\Lambda_{N1} + \Lambda_{N2}) = \bar{\bar{\mu}}\boldsymbol{\Lambda}_N$, while the corresponding post-impact velocities are zero. To find the unknown impulses in the normal $\boldsymbol{\Lambda}_N$ (vector) and the tangential direction Λ_T (scalar), the following system of coupled equations (7) must be solved:

$$\begin{aligned}\boldsymbol{\gamma}_N^+ &= \boldsymbol{\gamma}_N^- + \mathbf{G}_{NN}\boldsymbol{\Lambda}_N + \mathbf{G}_{NT}\Lambda_T + \bar{\bar{\varepsilon}}_N\boldsymbol{\gamma}_N^- = \mathbf{0} \\ \gamma_T^+ &= \gamma_T^- + \mathbf{G}_{TN}\boldsymbol{\Lambda}_N + G_{TT}\Lambda_T = 0 \end{aligned} \tag{47}$$

Adopting the proposed simulation (Fig. 8 bottom) and the corresponding definitions (40) and (41), this step is now trivial as no singular matrix is involved in the solution process. After some algebra the normal impulses and the tangential impulse are derived:

$$\begin{aligned}\boldsymbol{\Lambda}_N &= \frac{1}{G_{TT}-\mathbf{G}_{TN}\mathbf{G}_{NN}^{-1}\mathbf{G}_{NT}}\left[\mathbf{G}_{NN}^{-1}\mathbf{G}_{NT}\gamma_T^-\right. \\ &- \left[\mathbf{G}_{NN}^{-1}\mathbf{G}_{NT}\mathbf{G}_{TN}+(G_{TT}\right. \\ &\left.\left.- \mathbf{G}_{TN}\mathbf{G}_{NN}^{-1}\mathbf{G}_{NT})\mathbf{E}\right]\mathbf{G}_{NN}^{-1}(\bar{\bar{\varepsilon}}_N+\mathbf{E})\boldsymbol{\gamma}_N^-\right] \\ \Lambda_T &= \frac{\mathbf{G}_{TN}\mathbf{G}_{NN}^{-1}(\bar{\bar{\varepsilon}}_N+\mathbf{E})\boldsymbol{\gamma}_N^- - \gamma_T^-}{G_{TT}-\mathbf{G}_{TN}\mathbf{G}_{NN}^{-1}\mathbf{G}_{NT}} \end{aligned} \tag{48}$$

where product $\mathbf{G}_{TN}\mathbf{G}_{NN}^{-1}\mathbf{G}_{NT}$ yields a scalar value (see the Appendix).

Double stick, or double slip, occurs according to the following kinematical criteria for the pre-impact contact velocities:

$$\begin{aligned}&\left(\frac{\gamma_T^-}{\gamma_N^-}\right)_f < \frac{\gamma_T^-}{\gamma_N^-} < \left(\frac{\gamma_T^-}{\gamma_N^-}\right)_b \quad \text{stick} \\ &\frac{\gamma_T^-}{\gamma_N^-} \le \left(\frac{\gamma_T^-}{\gamma_N^-}\right)_f \quad \text{forward slip} \\ &\frac{\gamma_T^-}{\gamma_N^-} \ge \left(\frac{\gamma_T^-}{\gamma_N^-}\right)_b \quad \text{backward slip} \end{aligned} \tag{49}$$

where the two limit values are

$$\begin{aligned}\left(\frac{\gamma_T^-}{\gamma_N^-}\right)_f &= (1+\varepsilon_N)\frac{\mu+\frac{\bar{m}}{4}\frac{(L_1+L_2)^2}{I_1+I_2}\,\mathrm{c}\alpha(\mu\,\mathrm{c}\alpha-\mathrm{s}\alpha)}{1-\frac{\bar{m}}{4}\frac{(L_1+L_2)^2}{I_1+I_2}\,\mathrm{s}\alpha(\mu\,\mathrm{c}\alpha-\mathrm{s}\alpha)} \\ \left(\frac{\gamma_T^-}{\gamma_N^-}\right)_b &= (1+\varepsilon_N)\frac{\mu+\frac{\bar{m}}{4}\frac{(L_1+L_2)^2}{I_1+I_2}\,\mathrm{c}\alpha(\mu\,\mathrm{c}\alpha+\mathrm{s}\alpha)}{1+\frac{\bar{m}}{4}\frac{(L_1+L_2)^2}{I_1+I_2}\,\mathrm{s}\alpha(\mu\,\mathrm{c}\alpha+\mathrm{s}\alpha)} \end{aligned} \tag{50}$$

with: $\bar{m} = \frac{m_1 m_2}{m_1+m_2}$ and $\gamma_N^- < 0$.

Slip or stick at point 1 (Fig. 9(vii)–(ix)) The remaining impact states are in essence single impacts, since only one of the two contact points is active (i.e. $\Lambda_N > 0$ holds). The analysis is similar with the one in [1]. The normal impulse for backward (Fig. 9(vii)) or forward (Fig. 9(ix)) slip at point 1 is

$$\frac{\Lambda_{N1}}{\bar{m}\gamma_N^-} = -\frac{1}{\bar{m}} \frac{1+\varepsilon_N}{\frac{1}{\bar{m}} + \frac{r_{11}^2 \pm \mu r_{11} r_{T1}}{I_1} + \frac{r_{21}^2 \pm \mu r_{21} r_{T2}}{I_2}} \tag{51}$$

and the pertinent post-impact velocities:

$$\frac{\gamma_T^+}{\gamma_N^-} = \frac{\gamma_T^-}{\gamma_N^-} - \frac{\pm\frac{\mu}{\bar{m}} + \frac{r_{11} r_{T1} \pm \mu r_{T1}^2}{I_1} + \frac{r_{21} r_{T2} \pm \mu r_{T2}^2}{I_2}}{\frac{1}{\bar{m}} + \frac{r_{11}^2 - \mu r_{11} r_{T1}}{I_1} + \frac{r_{21}^2 - \mu r_{21} r_{T2}}{I_2}} \times (1+\varepsilon_N) \tag{52}$$

In (51) and (52), sign (+) holds for backward slip and sign (−) corresponds to forward slip. When stick takes place at point 1 (Fig. 9(viii)) the normal and tangential impulses are

$$\begin{aligned}
\frac{\Lambda_{N1}}{\bar{m}\gamma_N^-} &= \frac{1}{\bar{m}} \frac{(\frac{r_{11}r_{T1}}{I_1} + \frac{r_{21}r_{T2}}{I_2})\frac{\gamma_T^-}{\gamma_N^-} - (\frac{1}{\bar{m}} + \frac{r_{T1}^2}{I_1} + \frac{r_{T2}^2}{I_2})(1+\varepsilon_N)}{(\frac{1}{\bar{m}} + \frac{r_{11}^2}{I_1} + \frac{r_{21}^2}{I_2})(\frac{1}{\bar{m}} + \frac{r_{T1}^2}{I_1} + \frac{r_{T2}^2}{I_2}) - (\frac{r_{11}r_{T1}}{I_1} + \frac{r_{21}r_{T2}}{I_2})^2} \\
\frac{\Lambda_T}{\bar{m}\gamma_N^-} &= \frac{1}{\bar{m}} \frac{(\frac{r_{11}r_{T1}}{I_1} + \frac{r_{21}r_{T2}}{I_2})(1+\varepsilon_N) - (\frac{1}{\bar{m}} + \frac{r_{T1}^2}{I_1} + \frac{r_{T2}^2}{I_2})\frac{\gamma_T^-}{\gamma_N^-}}{(\frac{1}{\bar{m}} + \frac{r_{11}^2}{I_1} + \frac{r_{21}^2}{I_2})(\frac{1}{\bar{m}} + \frac{r_{T1}^2}{I_1} + \frac{r_{T2}^2}{I_2}) - (\frac{r_{11}r_{T1}}{I_1} + \frac{r_{21}r_{T2}}{I_2})^2}
\end{aligned} \tag{53}$$

For single impact at point 1, (49) holds, but the limits between slip and stick are

$$\begin{aligned}
\left(\frac{\gamma_T^-}{\gamma_N^-}\right)_f &= (1+\varepsilon_N)\frac{-\frac{\mu}{\bar{m}} + \frac{r_{11}r_{T1} - \mu r_{T1}^2}{I_1} + \frac{r_{21}r_{T2} - \mu r_{T2}^2}{I_2}}{\frac{1}{\bar{m}} + \frac{r_{11}^2 - \mu r_{11} r_{T1}}{I_1} + \frac{r_{21}^2 - \mu r_{21} r_{T2}}{I_2}} \\
\left(\frac{\gamma_T^-}{\gamma_N^-}\right)_b &= (1+\varepsilon_N)\frac{\frac{\mu}{\bar{m}} + \frac{r_{11}r_{T1} + \mu r_{T1}^2}{I_1} + \frac{r_{21}r_{T2} + \mu r_{T2}^2}{I_2}}{\frac{1}{\bar{m}} + \frac{r_{11}^2 + \mu r_{11} r_{T1}}{I_1} + \frac{r_{21}^2 + \mu r_{21} r_{T2}}{I_2}}
\end{aligned} \tag{54}$$

Slip or stick at point 2 (Fig. 9(iv)–(vi)) Similarly, the normal impulse for slip at point 2 is

$$\frac{\Lambda_{N2}}{\bar{m}\gamma_N^-} = -\frac{1}{\bar{m}} \frac{1+\varepsilon_N}{\frac{1}{\bar{m}} + \frac{r_{12}^2 \pm \mu r_{12} r_{T1}}{I_1} + \frac{r_{22}^2 \pm \mu r_{22} r_{T2}}{I_2}} \tag{55}$$

And the post-impact velocities:

$$\frac{\gamma_T^+}{\gamma_N^-} = \frac{\gamma_T^-}{\gamma_N^-} - \frac{\pm\frac{\mu}{\bar{m}} + \frac{r_{12} r_{T1} \pm \mu r_{T1}^2}{I_1} + \frac{r_{22} r_{T2} \pm \mu r_{T2}^2}{I_2}}{\frac{1}{\bar{m}} + \frac{r_{12}^2 - \mu r_{12} r_{T1}}{I_1} + \frac{r_{22}^2 - \mu r_{22} r_{T2}}{I_2}} \times (1+\varepsilon_N) \tag{56}$$

Again, in (55) and (56), sign (+) holds for backward slip (Fig. 9(iv)) and sign (−) corresponds to forward slip (Fig. 9(vi)). Also, (55) and (56) are the same as (51) and (52) if levers r_{12} and r_{22} are replaced with r_{11} and r_{21}, respectively.

The normal and tangential impulses for stick at point 2 (Fig. 9(v)) are

$$\begin{aligned}
\frac{\Lambda_{N2}}{\bar{m}\gamma_N^-} &= \frac{1}{\bar{m}} \frac{(\frac{r_{12}r_{T1}}{I_1} + \frac{r_{22}r_{T2}}{I_2})\frac{\gamma_T^-}{\gamma_N^-} - (\frac{1}{\bar{m}} + \frac{r_{T1}^2}{I_1} + \frac{r_{T2}^2}{I_2})(1+\varepsilon_N)}{(\frac{1}{\bar{m}} + \frac{r_{T1}^2}{I_1} + \frac{r_{T2}^2}{I_2})(\frac{1}{\bar{m}} + \frac{r_{12}^2}{I_1} + \frac{r_{22}^2}{I_2}) - (\frac{r_{12}r_{T1}}{I_1} + \frac{r_{22}r_{T2}}{I_2})^2} \\
\frac{\Lambda_T}{\bar{m}\gamma_N^-} &= \frac{1}{\bar{m}} \frac{(\frac{r_{12}r_{T1}}{I_1} + \frac{r_{22}r_{T2}}{I_2})(1+\varepsilon_N) - (\frac{1}{\bar{m}} + \frac{r_{12}^2}{I_1} + \frac{r_{22}^2}{I_2})\frac{\gamma_T^-}{\gamma_N^-}}{(\frac{1}{\bar{m}} + \frac{r_{T1}^2}{I_1} + \frac{r_{T2}^2}{I_2})(\frac{1}{\bar{m}} + \frac{r_{12}^2}{I_1} + \frac{r_{22}^2}{I_2}) - (\frac{r_{12}r_{T1}}{I_1} + \frac{r_{22}r_{T2}}{I_2})^2}
\end{aligned} \tag{57}$$

Table 1 Single frictional impact: equations and substitutions

$\theta_1^- - \theta_2^- < 0$ (e.g. $\theta_1^- = 0, \theta_2^- > 0$) 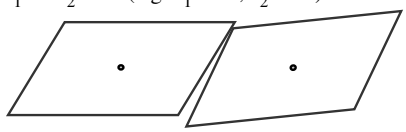	$\mathbf{r}_D^T \mathbf{t}_1 = 0$ (Case 1) $W_N \rightarrow$ from (18), $W_T \rightarrow$ from (19), $\sigma_2 = -W \tan\alpha\,/2$ and $\sigma_1 \rightarrow$ from (14)	Impact at point 1: levers in (51) to (53): $r_{11}, r_{21}, r_{T1}, r_{T2}$ correspond to: $\tilde{r}_{N1}, \tilde{r}_{N2}, \tilde{r}_{T1}, \tilde{r}_{T2}$ from (18), (19)
$\theta_1^- - \theta_2^- > 0$ (e.g. $\theta_1^- = 0, \theta_2^- < 0$) 	$\mathbf{r}_D^T \mathbf{t}_1 = 0$ (Case 1) $\mathbf{W}_N \rightarrow$ from (18), $\mathbf{W}_T \rightarrow$ from (19), $\sigma_2 = +W \tan\alpha\,/2$ and $\sigma_1 \rightarrow$ from (14)	Impact at point 2: levers in (55) to (57): $r_{12}, r_{22}, r_{T1}, r_{T2}$ correspond to: $\tilde{r}_{N1}, \tilde{r}_{N2}, \tilde{r}_{T1}, \tilde{r}_{T2}$ from (18), (19)
$\theta_1^- - \theta_2^- < 0$ (e.g. $\theta_1^- < 0, \theta_2^- = 0$) 	$\mathbf{r}_D^T \mathbf{t}_2 = 0$ (Case 2) $\mathbf{W}_N \rightarrow$ from (20), $\mathbf{W}_T \rightarrow$ from (21), $\sigma_1 = W \tan\alpha/2$, $\sigma_2 \rightarrow$ from (16)	Impact at point 1: levers in (51) to (53): r_{11}, r_{21}, r_{T1}, r_{T2} correspond to: $\tilde{r}_{N1}, \tilde{r}_{N2}, \tilde{r}_{T1}, \tilde{r}_{T2}$ from (20), (21)
$\theta_1^- - \theta_2^- > 0$ (e.g. $\theta_1^- > 0, \theta_2^- = 0$) 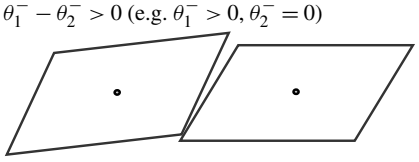	$\mathbf{r}_D^T \mathbf{t}_2 = 0$ (Case 2) $\mathbf{W}_N \rightarrow$ from (20), $\mathbf{W}_T \rightarrow$ from (21), $\sigma_1 = -W \tan\alpha/2$, $\sigma_2 \rightarrow$ from (16)	Impact at point 2: levers in (55) to (57): $r_{12}, r_{22}, r_{T1}, r_{T2}$ correspond to: $\tilde{r}_{N1}, \tilde{r}_{N2}, \tilde{r}_{T1}, \tilde{r}_{T2}$ from (20), (21)

For single impact at point 2 the velocity limits between slip and stick in (49) are given from (54) replacing r_{11} with r_{12} and r_{21} with r_{22}.

Synopsis In summary, two conditions govern the post-impact state of the frictional multi-impact problem of Fig. 8: (i) the geometrical and inertial conditions (31) determine which contact points are active (the pertinent normal impulse is positive $\Lambda_N > 0$) and (ii) the kinematical conditions (49) together with the contact parameters (ε_N and μ) determine whether the impact results in (forward/backward) slip or stick.

4.3 Single frictional impact

Single-impacts occur when the two bodies come in touch with different pre-impact rotations $\theta_1^- \neq \theta_2^-$ and/or different angular velocities. The proposed LCP (7), (8) describes also single frictional impacts, as a special case when only one impact point is active ($\Lambda_N > 0$ holds). In particular, the closed-form solutions of Sect. 4.2 for single-impact at point 1 (or point 2) are still valid provided the appropriate levers are used (see Table 1).

Figures 10 and 11 illustrate the existential conditions of the three different (frictional) post-impact states (forward slip, backward slip and stick) in the plane: pre-impact tangential and normal velocity ratio (γ_T^-/γ_N^-)—pre-impact rotation (θ^-). Both Figs. 10 and 11 concern bridges with skew angle $\alpha = 30^o$ and length ratios $L_1/L_2 = 2.0$ (top), 1.0 (middle), and 0.5 (bottom). Figure 10 covers the contact case $\mathbf{r}_D^T \mathbf{t}_2 = 0$, while Fig. 11 covers the case $\mathbf{r}_D^T \mathbf{t}_1 = 0$. For convenience, all results in Figs. 10 and 11 are based on the assumption that the impact point is located at a fixed distance from the nearest corner. In particular, for Fig. 10 it is assumed that $\sigma_2 = \pm 0.9 W \tan\alpha/2$ accordingly, whereas for Fig. 11 $\sigma_1 = \pm 0.9 W \tan\alpha/2$. This is just for practicality in order to specify a particular contact configuration among the infinite configurations covered with the same equations.

The tendency to stick (gray area in Figs. 10 and 11) increases with the coefficient of friction μ and with the difference in length of the two segments (directly related to the difference in mass). Systematically, the stick area is broader for impact near the obtuse corner of the shorter segment (with the lower mass). This ob-

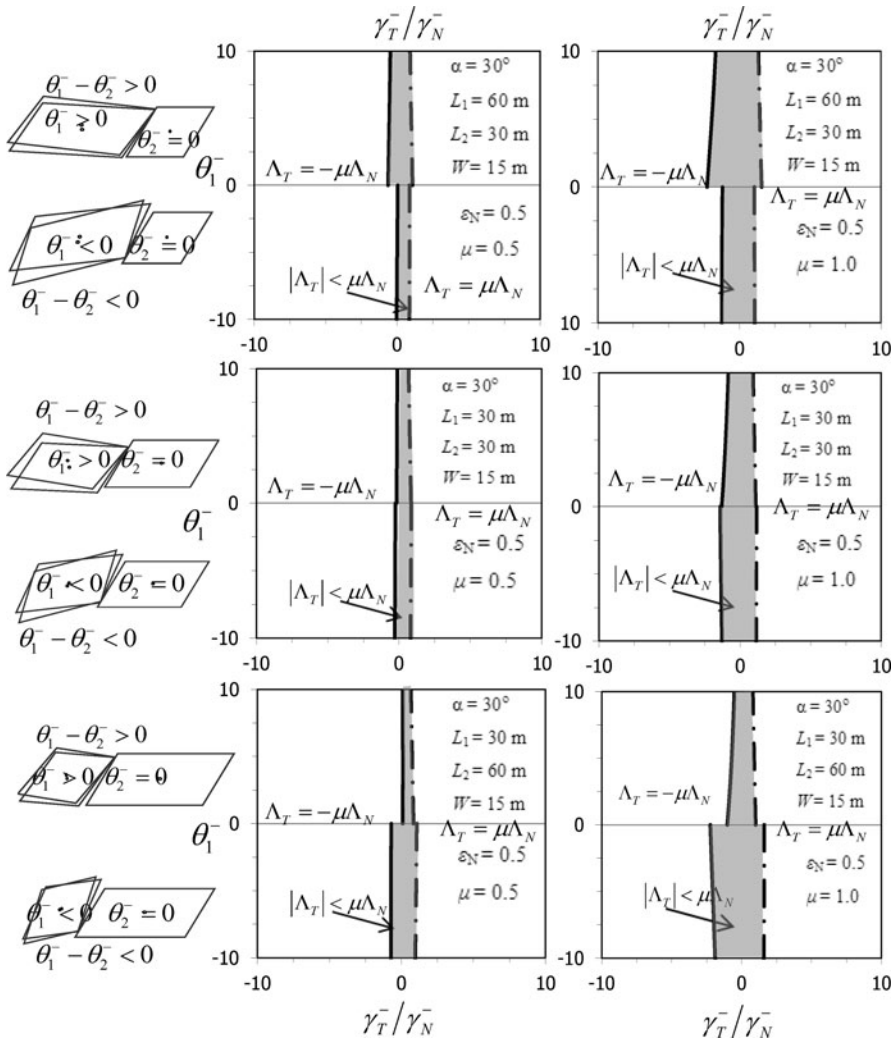

Fig. 10 The three distinct single (frictional) impact states in the $(\gamma_T^-/\gamma_N^- - \theta^-)$ plane, when $\theta_1^- \neq 0, \theta_2^- = 0$

servation is in agreement with the empirical observations that skew bridges tend to bind in their obtuse corners. A comprehensive analysis of the relative importance of all important parameters is beyond the scope of this paper. However, the present sample results offer a glimpse into the in-deck impact mechanism of skew bridges.

5 Conclusions

The present study examines the in-deck impact of multi-segment skew bridges; a lack of a thorough relevant study is observed in literature. It adopts a nonsmooth rigid body approach, combined with set-valued (contact) force laws, and analyzes in depth the impact response of a pair of planar skew (rigid) bodies.

Key feature of this analysis is a linear complementarity formulation which encapsulates all physically feasible post-impact states such as "stick", "slip" of single-point and double-point impact. The existential conditions and pertinent closed-form solutions of all post-impact states are derived. In the process, the paper proposes a rational way to avoid the appearance of singular matrices caused by dependent constraints.

The study shows that the geometry and the inertia properties define the active contact points, while the pre-impact kinematics and the contact parameters (the coefficient of restitution and the coefficient of friction) govern the behavior in the tangential direction of the

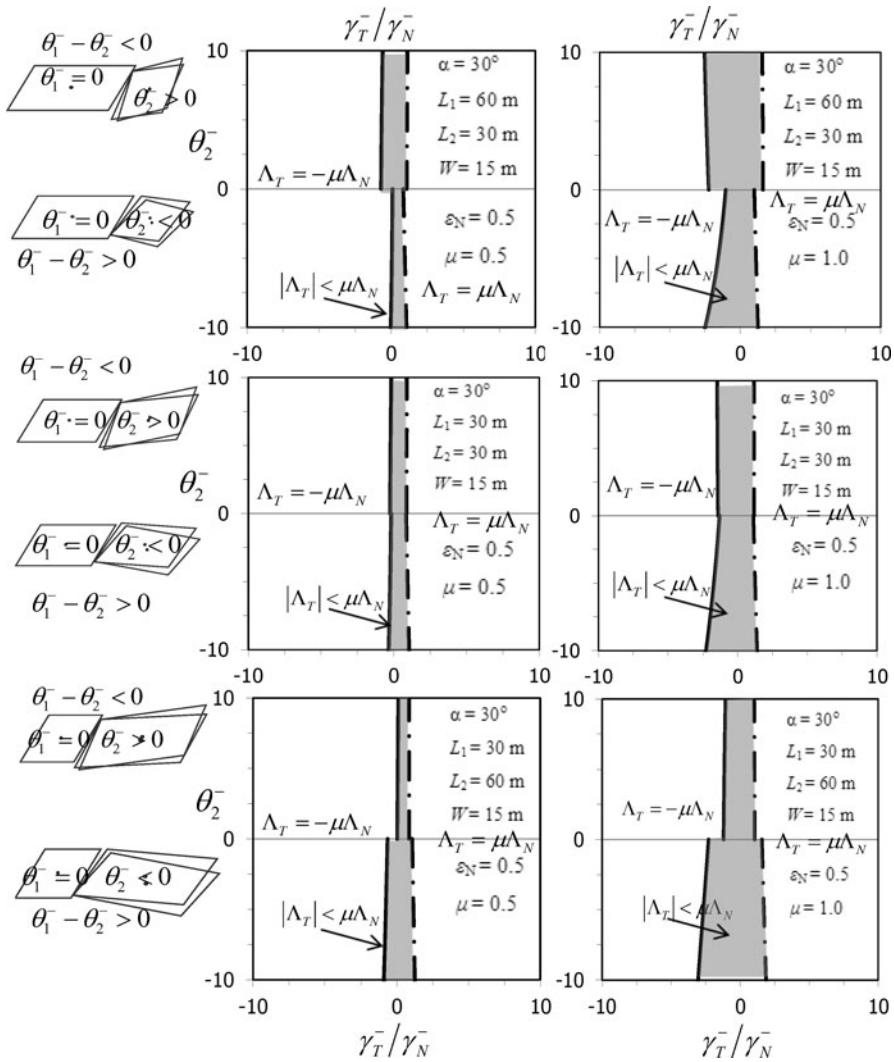

impact (slip or stick). The paper also offers equations which solve the contact kinematics between two adjacent skew planar rigid bodies and can be used to treat successively as many pairs of skew bridge-segments as necessary.

The results of this study confirm the empirically observed tendency of skew bridges to "stick" at the obtuse corner, and subsequently rotate in such a way that the skew angle increases. On the same time however, the study shows that the examined impact mechanism of two (skew) bodies configuration is overall considerably complicated and not adequately understood so far. Though the paper focuses on an impact problem of skew bridges, the adopted mechanical configuration and the proposed method of analysis might also be appropriate for different impact phenomena of more general interest.

Acknowledgements The author gratefully acknowledges the financial support for this research provided by the Research Grants Council of Hong Kong, under grant reference number DAG12EG03.

Appendix

The determinate $|\mathbf{G}_{NN}|$ is

$$|\mathbf{G}_{NN}| = \frac{(r_{11}r_{21} - r_{12}r_{22})^2}{I_1 I_2} + \left[\frac{(r_{11} - r_{12})^2}{I_1} + \frac{(r_{21} - r_{22})^2}{I_2}\right]\left(\frac{1}{m_1} + \frac{1}{m_2}\right) \tag{58}$$

The inverse of matrix $(\mathbf{G}_{NN} + \mathbf{G}_{NT}\bar{\bar{\boldsymbol{\mu}}})$ and its determinate D_1 can be written as

$$\begin{aligned}
&\left(\mathbf{G}_{NN} + \mathbf{G}_{NT}\bar{\bar{\boldsymbol{\mu}}}\right)^{-1} \\
&= \frac{1}{D_1}\begin{pmatrix} \frac{1}{m_1} + \frac{r_{12}^2 + \mu r_{12} r_{T1}}{I_1} + \frac{1}{m_2} + \frac{r_{22}^2 + \mu r_{22} r_{T2}}{I_2} & -\left(\frac{1}{m_1} + \frac{r_{11}r_{12} + \mu r_{11} r_{T1}}{I_1} + \frac{1}{m_2} + \frac{r_{21}r_{22} + \mu r_{21} r_{T2}}{I_2}\right) \\ -\left(1 + \frac{r_{11}r_{12} + \mu r_{12} r_{T1}}{I_1} + \frac{1}{m_2} + \frac{r_{21}r_{22} + \mu r_{22} r_{T2}}{I_2}\right) & \frac{1}{m_1} + \frac{r_{11}^2 + \mu r_{11} r_{T1}}{I_1} + \frac{1}{m_2} + \frac{r_{21}^2 + \mu r_{21} r_{T2}}{I_2} \end{pmatrix} \\
&D_1 = |\mathbf{G}_{NN} + \mathbf{G}_{NT}\bar{\bar{\boldsymbol{\mu}}}| = \frac{m_1 + m_2}{m_1 m_2}\left[\frac{(r_{11} - r_{12})^2}{I_1} + \frac{(r_{21} - r_{22})^2}{I_2}\right] \\
&\quad + \frac{r_{12}r_{21} - r_{11}r_{22}}{I_1 I_2}\left[\mu r_{T1}(r_{21} - r_{22}) + \mu r_{T2}(r_{12} - r_{11}) + r_{12}r_{21} - r_{11}r_{22}\right]
\end{aligned} \tag{59}$$

Similarly for the inverse of matrix $(\mathbf{G}_{NN} - \mathbf{G}_{NT}\bar{\bar{\boldsymbol{\mu}}})$ and its determinate D_2, we have

$$\begin{aligned}
&\left(\mathbf{G}_{NN} - \mathbf{G}_{NT}\bar{\bar{\boldsymbol{\mu}}}\right)^{-1} \\
&= \frac{1}{D_2}\begin{pmatrix} \frac{1}{m_1} + \frac{1}{m_2} + \frac{r_{12}^2 - \mu r_{12} r_{T1}}{I_1} + \frac{r_{22}^2 - \mu r_{22} r_{T2}}{I_2} & -\left(\frac{1}{m_1} + \frac{1}{m_2} + \frac{r_{11}r_{12} - \mu r_{11} r_{T1}}{I_1} + \frac{r_{21}r_{22} - \mu r_{21} r_{T2}}{I_2}\right) \\ -\left(\frac{1}{m_1} + \frac{1}{m_2} + \frac{r_{11}r_{12} - \mu r_{12} r_{T1}}{I_1} + \frac{r_{21}r_{22} - \mu r_{22} r_{T2}}{I_2}\right) & \frac{1}{m_1} + \frac{1}{m_2} + \frac{r_{11}^2 - \mu r_{11} r_{T1}}{I_1} + \frac{r_{21}^2 - \mu r_{21} r_{T2}}{I_2} \end{pmatrix} \\
&D_2 = |\mathbf{G}_{NN} - \mathbf{G}_{NT}\bar{\bar{\boldsymbol{\mu}}}| = \frac{m_1 + m_2}{m_1 m_2}\left[\frac{(r_{11} - r_{12})^2}{I_1} + \frac{(r_{21} - r_{22})^2}{I_2}\right] \\
&\quad + \frac{r_{12}r_{21} - r_{11}r_{22}}{I_1 I_2}\left[\mu r_{T1}(r_{22} - r_{21}) + \mu r_{T2}(r_{11} - r_{12}) + r_{12}r_{21} - r_{11}r_{22}\right]
\end{aligned} \tag{60}$$

For $\mu = 0$ (59) and (60) reduce to (26) and (58) of frictionless collisions.
Finally, the product $\mathbf{G}_{TN}\mathbf{G}_{NN}^{-1}\mathbf{G}_{NT}$ returns the scalar value:

$$\begin{aligned}
&\mathbf{G}_{TN}\mathbf{G}_{NN}^{-1}\mathbf{G}_{NT} \\
&= \frac{1}{|\mathbf{G}_{NN}|}\left[\left(\frac{1}{m_1} + \frac{1}{m_2}\right)\left(\frac{r_{11} - r_{12}}{I_1}r_{T1} + \frac{r_{21} - r_{22}}{I_2}r_{T2}\right)^2 + \left(\frac{r_{T1}^2}{I_1} + \frac{r_{T2}^2}{I_2}\right)\frac{(r_{11}r_{22} - r_{12}r_{21})^2}{I_1 I_2}\right]
\end{aligned} \tag{61}$$

References

1. Dimitrakopoulos, E.G.: Analysis of a frictional oblique impact observed in skew bridges. Nonlinear Dyn. **60**, 575–595 (2010)
2. Dimitrakopoulos, E.G., Makris, N., Kappos, A.J.: Dimensional analysis of the earthquake-induced pounding between adjacent structures. Earthq. Eng. Struct. Dyn. **38**(7), 867–886 (2009)
3. Dimitrakopoulos, E.G., Makris, N., Kappos, A.J.: Dimensional analysis of the earthquake response of a pounding oscillator. J. Eng. Mech. **136**(3), 299–310 (2010)
4. EERL (Earthquake Engineering Research Laboratory): In: Jennings, P.C. (ed.) Engineering Features of the San Fernando Earthquake of February 9, 1971. California Institute of Technology, Pasadena (1971)
5. Elnashai, A.S., Gencturk, B., Kwon, O.S., Hashash, Y.M.A., Kim, S.J., Jeong, S.-H., Dukes, J.: The Maule (Chile) earthquake of February 27, 2010: development of hazard, site specific ground motions and back-analysis of structures. Soil Dyn. Earthq. Eng. **42**, 229–245 (2012)
6. Zhang, H., Li, J., Saiidi, S.: Evaluation of performance of a skew bridge in Wenchuan 2008 earthquake. In: Proceedings of the International Symposium on Engineering Lessons Learned from the 2011 Great. East Japan Earthquake, Tokyo, Japan (2012)
7. Kaviani, P., Zareian, F., Taciroglu, E.: Seismic behavior of reinforced concrete bridges with skew-angled seat-type abutments. Eng. Struct. **45**, 137–150 (2012)
8. Kalantari, A., Amjadian, M.: An approximate method for dynamic analysis of skewed highway bridges with continuous rigid deck. Eng. Struct. **32**(9), 2850–2860 (2010)

9. Meng, J., Lui, E.M.: Torsional effects on short-span highway bridges. Comput. Struct. **75**(6), 619–629 (2000)
10. He, X.H., Sheng, X.W., Scanlon, A., Linzell, D.G., Yu, X.D.: Skewed concrete box girder bridge static and dynamic testing and analysis. Eng. Struct. **39**, 38–49 (2012)
11. Robson, B.N., Harik, I.E., Gupta, V.: Effectiveness of seismic isolation of highly skewed P/C I-girder bridge. J. Bridge Eng. **6**(3), 221–224 (2001)
12. Priestley, M.J.N., Calvi, G.M., Seible, F.: Seismic Design and Retrofit of Bridges. Wiley, New York (1996)
13. Kawashima, K., Unjoh, S., Hoshikuma, J., Kosa, K.: Damage of transportation facility due to 2010 Chile earthquake (April 5 2010). Bridge team dispatched by Japan society of civil engineers (2010). http://peer.berkeley.edu/events/pdf/2010/Bridge_Damage_by_Chile_EQ_JSCE_Team.pdf
14. Huo, Y., Zhang, J.: Effects of pounding and skewness on seismic responses of typical multi-span highway bridges using fragility function method. J. Bridge Eng. (2012). doi:10.1061/(ASCE)BE.1943-5592.0000414
15. Taflanidis, A.A.: Optimal probabilistic design of seismic dampers for the protection of isolated bridges against near-fault seismic excitations. Eng. Struct. **33**(12), 3496–3508 (2011)
16. Dimitrakopoulos, E.G., Makris, N., Kappos, A.J.: Dimensional analysis of the earthquake-induced pounding between inelastic structures. Bull. Earthq. Eng. **9**(2), 561–579 (2011)
17. Sevgili, G., Caner, A.: Improved seismic response of multisimple-span skewed bridges retrofitted with link slabs. J. Bridge Eng. **14**(6), 452–459 (2009)
18. Maragakis, E.A., Jennings, P.C.: Analytical models for the rigid body motions of skew bridges. Earthq. Eng. Struct. Dyn. **15**(8), 923–944 (1987)
19. Tirasit, P., Kawashima, K.: Effect of nonlinear seismic torsion on the performance of skewed bridge piers. J. Earthq. Eng. **12**(6), 980–998 (2008)
20. Bignell, J., Lafave, J., Hawkins, N.: Seismic vulnerability assessment of wall pier supported highway bridges using nonlinear pushover analyses. Eng. Struct. **27**(14), 2044–2063 (2005)
21. Abdel-Mohti, A., Pekcan, G.: Seismic response of skewed RC box-girder bridges. Earthq. Eng. Eng. Vib. **7**(4), 415–426 (2008)
22. Maleki, S.: Seismic modeling of skewed bridges with elastomeric bearings and side retainers. J. Bridge Eng. **10**(4), 442–449 (2005)
23. Saadeghvaziri, M., Yazdanimotlagh, A.: Seismic behavior and capacity/demand analyses of three multi-span simply supported bridges. Eng. Struct. **30**(1), 54–66 (2008)
24. Watanabe, G., Kawashima, K.: Effectiveness of cable-restrainer for mitigating rotation of a skewed bridge subjected to strong ground shaking. In: 13th World Conference on Earthquake Engineering, Vancouver, BC, Canada (2004). Paper No. 789
25. EERI Earthquake Engineering Research Institute. The Tehuacan, Mexico, Earthquake of June 15, 1999. EERI, Oakland, California (1999)
26. Brogliato, B.: Nonsmooth Mechanics: Models, Dynamics and Control, 2nd edn. Springer, New York (1999)
27. Glocker, C.: Set-Valued Force Laws: Dynamics of Non-smooth Systems. Springer, New York (2001)
28. Mistakidis, E., Stavroulakis, G.E.: Nonconvex Optimization in Mechanics: Algorithms, Heuristics, and Engineering Applications by the F.E.M. Kluwer Academic, Boston (1998)
29. Pfeiffer, F., Glocker, C.: Multibody Dynamics with Unilateral Contacts. Wiley/VCH, Weinheim (2004)
30. Panagiotopoulos, P.D.: Dynamic and incremental variational inequality principles, differential inclusions and their applications to co-existent phases problems. Acta Mech. **40**(1–2), 85–107 (1981)
31. Payr, M., Glocker, C.: Oblique frictional impact of a bar: analysis and comparison of different impact laws. Nonlinear Dyn. **41**(4), 361–383 (2005)
32. Flores, P., Leine, R., Glocker, C.: Application of the non-smooth dynamics approach to model and analysis of the contact-impact events in cam-follower systems. Nonlinear Dyn. **69**(4), 2117–2133 (2012)
33. Dimitrakopoulos, E.G.: Seismic response analysis of skew bridges with pounding deck–abutment joints. Eng. Struct. **33**(3), 813–826 (2011)